To Sue

From Zoe

Date March 28, 1989

memo

University of Waterloo

Sue:

Would you go ahead and have 50 run off in the Math covers please - 126-6041-41.

Please return the originals after printing to Peter. You can sign the req.

Thanks,

z

Make a copy for me for my files.

Printing Requisition / Graphic Services

60809

1. **Please complete unshaded areas** on form as applicable.
2. **Distribute copies** as follows: White and Yellow to Graphic Services. **Retain Pink Copies for your records.**
3. On completion of order the **Yellow copy will be returned** with the printed material.
4. Please direct enquiries, quoting requisition number and account number, to extension 3451.

TITLE OR DESCRIPTION

Radioactive Waste Disposal Heating Effects in Unsaturated Fractured Rock CS-89-10

DATE REQUISITIONED	DATE REQUIRED	ACCOUNT NO.
March 29/89	ASAP	1 2 6 6 0 4 1 4 1

REQUISITIONER – PRINT	PHONE	SIGNING AUTHORITY
P. Forsyth	4415	S. DeAngelis / P. Forsyth

MAILING INFO –	NAME	DEPT.	BLDG. & ROOM NO.	
	Sue DeAngelis	C.S.	DC 2314	X DELIVER ☐ PICK-UP

Copyright: I hereby agree to assume all responsibility and liability for any infringement of copyrights and/or patent rights which may arise from the processing of, and reproduction of, any of the materials herein requested. I further agree to indemnify and hold blameless the University of Waterloo from any liability which may arise from said processing or reproducing. I also acknowledge that materials processed as a result of this requisition are for educational use only.

NUMBER OF PAGES: 66 NUMBER OF COPIES: 50

TYPE OF PAPER STOCK
☒ BOND ☐ NCR ____ PT. ☒ COVER ☐ BRISTOL ☒ SUPPLIED ☐ ____

PAPER SIZE
☒ 8½ x 11 ☐ 8½ x 14 ☐ 11 x 17 ☐ ____

PAPER COLOUR: ☒ WHITE ☐ ____ INK: ☒ BLACK ☐ ____

PRINTING: ☐ 1 SIDE ____ PGS. ☒ 2 SIDES ____ PGS. NUMBERING: FROM ____ TO ____

BINDING/FINISHING: 3 down left side
☒ COLLATING ☒ STAPLING ☐ ____ HOLE PUNCHED ☐ PLASTIC RING

FOLDING/PADDING: CUTTING SIZE:

Special Instructions

Math fronts and backs enclosed.

COPY CENTRE — OPER. NO. | BLDG. | MACH. NO.

DESIGN & PASTE-UP — OPER. NO. | TIME | LABOUR CODE

			D 0 1
			D 0 1
			D 0 1

TYPESETTING — QUANTITY | OPER. NO. | TIME | LABOUR CODE

PAP 0 0 0 0 0 0				T 0 1
PAP 0 0 0 0 0 0				T 0 1
PAP 0 0 0 0 0 0				T 0 1

PROOF

PRF				
PRF				
PRF				

NEGATIVES — QUANTITY | OPER. NO. | TIME | LABOUR CODE

FLM				C 0 1
FLM				C 0 1
FLM				C 0 1
FLM				C 0 1
FLM				C 0 1

PMT

PMT				C 0 1
PMT				C 0 1
PMT				C 0 1

PLATES

PLT				P 0 1
PLT				P 0 1
PLT				P 0 1

STOCK

				0 0 1
				0 0 1
				0 0 1
				0 0 1

BINDERY

RNG				B 0 1
RNG				B 0 1
RNG				B 0 1
MIS 0 0 0 0 0				B 0 1

OUTSIDE SERVICES

$____ COST

TAXES – PROVINCIAL ☐ FEDERAL ☐

GRAPHIC SERV. OCT. 86 482-2

Printing Requisition / Graphic Services

60809

1. **Please complete unshaded areas** on form as applicable.
2. **Distribute copies** as follows: White and Yellow to Graphic Services. **Retain Pink Copies for your records.**
3. On completion of order the **Yellow copy will be returned** with the printed material.
4. Please direct enquiries, quoting requisition number and account number, to extension 3451.

TITLE OR DESCRIPTION

Radioactive Waste Disposal Heating Effects in Unsaturated Fractured Rock CS-89-10

DATE REQUISITIONED	DATE REQUIRED	ACCOUNT NO.
March 29/89	ASAP	1 2 6 6 0 4 1 4 1

REQUISITIONER – PRINT	PHONE	SIGNING AUTHORITY
P. Forsyth	4415	S. DeAngelis / P. Forsyth

MAILING INFO –	NAME	DEPT.	BLDG. & ROOM NO.	
	Sue DeAngelis	C.S.	DC 2314	X DELIVER ☐ PICK-UP

Copyright: I hereby agree to assume all responsibility and liability for any infringement of copyrights and/or patent rights which may arise from the processing of, and reproduction of, any of the materials herein requested. I further agree to indemnify and hold blameless the University of Waterloo from any liability which may arise from said processing or reproducing. I also acknowledge that materials processed as a result of this requisition are for educational use only.

NUMBER OF PAGES 66 NUMBER OF COPIES 50

TYPE OF PAPER STOCK
☒ BOND ☐ NCR ____ PT. ☒ COVER ☐ BRISTOL ☒ SUPPLIED ☐ ____

PAPER SIZE
☒ 8½ x 11 ☐ 8½ x 14 ☐ 11 x 17 ☐ ____

PAPER COLOUR ☒ WHITE ☐ ____ INK ☒ BLACK ☐ ____

PRINTING ☐ 1 SIDE ____ PGS. ☒ 2 SIDES ____ PGS. NUMBERING FROM ____ TO ____

BINDING/FINISHING 3 down left side
☒ COLLATING ☒ STAPLING ☐ ____ HOLE PUNCHED ☐ PLASTIC RING

FOLDING/PADDING ____ CUTTING SIZE ____

Special Instructions

Math fronts and backs enclosed.

COPY CENTRE OPER. NO. ____ BLDG. ____ MACH. NO. ____

DESIGN & PASTE-UP

OPER. NO.	TIME	LABOUR CODE
		D01
		D01
		D01

TYPESETTING

	QUANTITY	OPER. NO.	TIME	LABOUR CODE
PAP000000				T01
PAP000000				T01
PAP000000				T01

PROOF

PRF				
PRF				
PRF				

NEGATIVES

	QUANTITY	OPER. NO.	TIME	LABOUR CODE
FLM				C01
FLM				C01
FLM				C01
FLM				C01
FLM				C01

PMT

PMT				C01
PMT				C01
PMT				C01

PLATES

PLT				P01
PLT				P01
PLT				P01

STOCK

				001
				001
				001
				001

BINDERY

RNG				B01
RNG				B01
RNG				B01
MIS000000				B01

OUTSIDE SERVICES

$____ COST

TAXES – PROVINCIAL ☐ FEDERAL ☐

GRAPHIC SERV. OCT. 85 482-2

Radioactive Waste Disposal Heating Effects in Unsaturated Fractured Rock

by

P.A. Forsyth

Research Report CS-89-10

Faculty of Mathematics

University of Waterloo
Waterloo, Ontario, Canada
N2L 3G1

Radioactive Waste Disposal Heating Effects in Unsaturated Fractured Rock

by

P.A. Forsyth

Research Report CS-89-10
February 1989

Radioactive Waste Disposal Heating Effects in Unsaturated Fractured Rock

P.A. Forsyth
University of Waterloo
Department of Computer Science
Waterloo, Ontario N2L 3G1

Running Title: Heating Effects in Unsaturated Rock
Keywords: Porous medium, two phase flow, variable substitution
Subject Classification: 65M05, 76505

ABSTRACT

Numerical techniques are described for modelling two phase (liquid and gas), two component (water and air) non-isothermal flow in fractured porous media. Interphase mass transfer, latent heat, conduction, convection, gravity and capillary effects are included. A rigorous method based on variable substitution is described to circumvent numerical problems associated with phase disappearance/appearance. Test calculations show that selection of primary variables for the Newton iteration has a profound effect on the number of nonlinear iterations required for convergence. Comparisons with previously reported computations indicate that the method used here is very efficient. For a fractured waste canister problem, a previously unreported pressure pulse phenomenon is predicted. Comparisons of one and two dimensional simulations show that one dimensional results can be misleading.

1. Introduction

Many industrial and geological processes involve multi-phase heat and mass transfer in a porous medium. Examples of such processes are drying of porous solids [1], geothermal energy production [2], post accident boiling of fluids in nuclear reactor debris [3], and nuclear waste disposal [4-8]. In many cases of interest, boiling of fluids occurs, and and both liquid and gaseous phases are present. Consequently, heat transfer takes place through the mechanisms of conduction, convection, and latent heats of vaporization and condensation.

A particularly efficient method of heat transfer occurs in a heat pipe [8-9]. A heat pipe is formed when a heat source causes vaporization of a volatile liquid, and consequent pressure build-up in the gaseous phase. This results in gas phase flow away from the heat source to cooler regions. The vapour then condenses in the cool region. Consequently, latent heat is transported away from the heat source with a relatively small temperature gradient. Gravitational and capillary forces provide a continuous flow of liquid back to the heat source.

In this article, a numerical model is developed for two phase (liquid and gas), two component (air and water), heat and mass transfer in a porous medium. Interphase mass transfer, latent heat, conduction, convection, diffusion, gravity and capillary effects are included. The numerical techniques are quite general, and can be used for any type of multi-phase heat and mass transfer problem in a porous medium, and for any number of dimensions.

In particular, attention is focussed on the problem of heat pipe effects which occur near high-level nuclear waste packages buried in a partially saturated porous material. A double porosity - double permeability approach is used to model fractured rock.

Several authors have proposed one-dimensional, semi-analytic methods for this problem [8-9]. Full numerical solutions have also been reported for single porosity systems [4-8]. The fractured rock case has been simulated in an approximate manner using an "effective continuum" approach [7-8], although a full numerical computation has been used to justify the effective continuum method [10]. The dual porosity - dual permeability approach results in a difficult numerical problem because of the small fracture pore volumes and very large capillary pressures typically encountered [10].

In this paper, a variable substitution method is described for handling the problem of phase appearance and disappearance (dry out, boiling, condensation). Since the discrete equations are highly non-linear due to thermodynamic phase equilibria

conditions, full Newton iteration is used. Some discussion will be presented which addresses the issue of methods for ensuring good convergence of the Newton iteration. When large capillary pressures are encountered, the choice of primary variables can have a dramatic effect on convergence behaviour.

Numerical results are presented for one and two dimensional problems. The one dimensional results are compared with previously obtained semi-analytic and numerical predictions, where available. Some interesting phenomena occur in the case of fractured rock. To the best of our knowledge, these phenomena have not been reported previously. This effect is a result of non-equilibrium between gas phase pressures in the fractures and the rock matrix. Consequently, this effect cannot be predicted using an effective continuum approach.

2. Formulation

In common with previous authors [1-11], we will assume the validity of the multiphase form of Darcy's law. Instantaneous thermal equilibrium between phases will also be assumed. Note that we will not assume instantaneous equilibrium between rock matrix and fracture pressures.

To avoid a profusion of subscripts, the equations will first be described for a single porosity system. The conservation equations for a two phase (ℓ-liquid, g-gas) air water (a-air, w-water) system are:

Conservation of air:

$$\frac{\partial}{\partial t}\left(\phi\left[S_\ell M_\ell X_a + S_g M_g Y_a\right]\right) \tag{1}$$

$$= \nabla\cdot\left\{M_\ell X_a \frac{K K_{r\ell}}{\mu_\ell} \nabla\psi_\ell\right\}$$

$$+ \nabla\cdot\left\{M_g Y_a \frac{K K_{rg}}{\mu_g} \nabla\psi_g\right\}$$

$$+ \nabla\cdot\left\{D_g M_g \nabla Y_a\right\}$$

$$+ M_g Y_a q_g' + M_\ell X_a q_\ell'$$

Conservation of water:

$$\frac{\partial}{\partial t}(\phi[S_\ell M_\ell X_w + S_g M_g Y_w]) \tag{2}$$

$$= \nabla \cdot \{M_\ell X_w \frac{K K_{r\ell}}{\mu_\ell} \nabla \psi_\ell\}$$

$$+ \nabla \cdot \{M_g Y_w \frac{K K_{rg}}{\mu_g} \nabla \psi_g\}$$

$$+ \nabla \cdot \{D_g M_g \nabla Y_w\}$$

$$+ M_g Y_w q_g' + M_\ell X_w q_\ell'$$

Conservation of energy:

$$\frac{\partial}{\partial t}(\phi[S_\ell M_\ell U_\ell + S_g M_g U_g]$$

$$+ (1-\phi) U_r M_r)$$

$$= \nabla \cdot \{h_\ell M_\ell \frac{K K_{r\ell}}{\mu_\ell} \nabla \psi_\ell\}$$

$$+ \nabla \cdot \{h_g M_g \frac{K K_{rg}}{\mu_g} \nabla \psi_g\}$$

$$+ \nabla \cdot \{D_g M_g h_{gw} \nabla Y_w\}$$

$$+ \nabla \cdot \{D_g M_g h_{ga} \nabla Y_a\}$$

$$+ M_g h_g q_g' + M_\ell h_\ell q_\ell'$$

$$+ \nabla \cdot \lambda \nabla T + q_{en}'$$

The phase potential gradients are given by:

$$\nabla \psi_m = \nabla P_m - \rho_m g \nabla D \tag{3}$$

where:

S_m = saturation of phase $m = \ell, g$

P_m = pressure of phase m $[Kpa]$

T = temperature $[^\circ K]$

K = absolute permeability $[m^2]$

K_{rm} = relative permeability of phase m

μ_m = viscosity of phase m [Kpa-day]

U_m = internal energy of phase m (r=rock) [J/mole]

h_m = enthalpy of phase m [J/mole]

M_m = molar density of phase m [mole/m^3]

q_m' = volumetric source/sink term for phase $m = \ell, g$ [$m^3/(m^3 -$ day)]

q_{en}' = source/sink term for energy [$J/(m^3 -$ day)]

ϕ = porosity

λ = heat conductivity [$J/(m$-day-$^\circ K$)]

D_g = gas phase diffusivity [m^2/day]

ρ_m = mass density of phase m [Kg/m^3]

g = acceleration due to gravity

D = depth [m]

Y_p = mole fraction of component p in the gas phase

X_p = mole fraction of component p in the liquid phase

In keeping with previous work, [4-9] we have ignored thermal dispersion effects, and considered only molecular diffusion in the gas phase. Note that we have assumed that $X_a \neq 0$, i.e. that a small amount of air is dissolved in the liquid phase. Of course, the small amount of X_a has no real effect in practical situations, but it is a useful numerical device to ensure that phase appearance/disappearance is handled smoothly. This will be discussed in a later section.

3. Fractured Rock Equations

If the rock matrix has only a small number of fractures, these can be modelled individually. However, in most situations, it would be impractical to do this, since the number of fractures in any reasonably sized computational control volume is very large. The orientation, size and distribution of the fractures is also more or less randomly distributed. Consequently, in order to take into account the fractures, the dual-porosity model is frequently employed [11-13]. Essentially, the rock matrix and fractures are treated as separate continua throughout the region of interest. Every

point contains fracture variables and matrix variables, and fluid may flow through fractures and matrix. The two continua are connected by a fluid and heat exchange term [11-13].

Consequently, the differential equations for a dual porosity - dual permeability model would be two sets of equations (1-3), one for the rock matrix and one for the fractures. The fluid exchange terms could be represented by source/sink terms. However, since the exchange terms have the form similar to the usual flow terms, it is in fact easier to write down the discretized equations (1-3) in a general way, and then all flow/exchange terms are treated in a very natural manner.

Consider discretizing equations (1-3) using a finite-volume technique [14-16]. First, control volumes must be defined. In general, the control volumes can have any type of shape (quadrilateral, triangular, etc). It is also assumed that within each control volume, there are many fractures, as shown in Figure 1. A more detailed discussion of dual porosity formulations can be found in [11].

Consequently, equations (1-3) can be discretized in the following way:

Conservation of air:

$$
\begin{aligned}
&\{(\phi\,[S_\ell\, M_\ell\, X_a + S_g\, M_g\, Y_a])^{N+1} \\
&-(\phi\,[S_\ell\, M_\ell\, X_a + S_g\, M_g\, Y_a])^{N}\,\}\,\frac{V_i}{\Delta t} \\
&=(M_g\, Y_a\, q_g)_i^{N+1} + (M_\ell\, X_a\, q_\ell)_i^{N+1} \\
&+\sum_{j\,\epsilon\,\eta_i} \gamma_{ij}\,\{(M_\ell\, X_a\, \frac{K_{r\ell}}{\mu_\ell}\,)_{jup}^{N+1}\, K_{j+\frac{1}{2}}\,[(P_{\ell j}^{N+1} - P_{\ell i}^{N+1}) \\
&\qquad\qquad -\rho_{\ell\, j+\frac{1}{2}}^{N+1}\, g(D_j - D_i)] \\
&+(M_g\, Y_a\, \frac{K_{rg}}{\mu_g}\,)_{jup}^{N+1}\, K_{j+\frac{1}{2}}\,[(P_{gj}^{N+1} - P_{gi}^{N+1}) \\
&\qquad\qquad -\rho_{gj+\frac{1}{2}}^{N+1}\, g(D_j - D_i)] \\
&+(D_g\, M_g)_{j+\frac{1}{2}}^{N+1}\,(Y_{aj}^{N+1} - Y_{ai}^{N+1})\}
\end{aligned}
\tag{4}
$$

Conservation of water:

$$\{(\phi\,[S_\ell\,M_\ell\,X_w + S_g\,M_g\,Y_w])^{N+1} \tag{5}$$

$$-(\phi\,[S_\ell\,M_\ell\,X_w + S_g\,M_g\,Y_w])^{N}\}\frac{V_i}{\Delta t}$$

$$= (M_g\,Y_w\,q_g)^{N+1} + (M_\ell\,X_w\,q_\ell)^{N+1}$$

$$+ \sum_{j\epsilon\eta_i} \gamma_{ij}\,\{(M_\ell\,X_w\,\frac{K_{r\ell}}{\mu_\ell})^{N+1}_{jup}\,K_{j+\frac{1}{2}}\,[(P^{N+1}_{\ell j} - P^{N+1}_{\ell i})$$

$$-\rho^{N+1}_{\ell\,j+\frac{1}{2}}\,g(D_j - D_i)]$$

$$+(M_g\,Y_w\frac{K_{rg}}{\mu_g})^{N+1}_{jup}\,K_{\,j+\frac{1}{2}}[(P^{N+1}_{gj} - P^{N+1}_{gi})$$

$$-\rho^{N+1}_{gj+\frac{1}{2}}\,g(D_j - D_i)]$$

$$+(D_g\,M_g)^{N+1}_{j+\frac{1}{2}}\,(Y^{N+1}_{wj} - Y^{N+1}_{wi})\}$$

Conservation of energy:

$$\{(\phi\,[S_\ell\,M_\ell\,U_\ell + S_g\,M_g\,U_g])^{N+1} \tag{6}$$

$$+[(1-\phi)\,U_r\,M_r]^{N+1} - (\phi\,[S_\ell\,M_\ell\,U_\ell + S_g\,M_g\,U_g])^{N}$$

$$-[(1-\phi)\,U_r\,M_r]^{N}\}\,\frac{V_i}{\Delta t}$$

$$= (M_g\,h_g\,q_g)^{N+1} + (M_\ell\,h_\ell\,q_\ell)^{N+1} + q^{N+1}_{\ell n}$$

$$+ \sum_{j\epsilon\eta_i} \gamma_{ij}\,\{(h_\ell\,M_\ell\,\frac{K_{r\ell}}{\mu_\ell})^{N+1}_{jup}\,K_{k+\frac{1}{2}}\,[(P^{N+1}_{\ell j} - P^{N+1}_{\ell j})$$

$$-\rho^{N+1}_{\ell\,j+\frac{1}{2}}\,g(D_j - D_i)]$$

$$+(h_g\,M_g\,\frac{K_{rg}}{\mu_g})^{N+1}_{jup}\,K_{j+\frac{1}{2}}\,[(P^{N+1}_{gj} - P^{N+1}_{gi}) - \rho^{N+1}_{gj+\frac{1}{2}}\,g(D_j - D_i)]$$

$$+(D_g\,M_g\,h_{gw})^{N+1}_{j+\frac{1}{2}}\,(Y^{N+1}_{wj} - Y^{N+1}_{wi})$$

$$+(D_g\,M_g\,h_{ga})^{N+1}_{j+\frac{1}{2}}\,(Y^{N+1}_{aj} - Y^{N+1}_{ai})$$

$$+\lambda^{N+1}_{j+\frac{1}{2}}\,(T^{N+1}_j - T^{N+1}_i)\}$$

where η_i is the set of neighbours of node i. For example, if rectangular cells are used for a single porosity problem, then η_i would be $\{i-1, i+1\}$ in one dimension. The geometric factor γ_{ij} will depend on the dimensionality, co-ordinate system, and whether the nodes $\{i, j\}$ are in the same porosity continuum. The source/sink terms have been renormalized:

$$q_m = q_m' V_i$$

$$q_{en} = q_{en}' V_i$$

where V_i is the volume of the i^{th} finite volume.

Equations (4-6) are valid for any number of dimensions, and for single and double porosity problems. (Note that for fractures, the rock heat capacity term in equation (6) is zero). If a single porosity system is being modelled, η_i is the set of geometric neighbours, in which case:

$$\gamma_{ij} = \frac{A_{ij}}{\Delta x_{ij}} \tag{7}$$

for rectangular geometry. In equation (7), A_{ij} is the interfacial area between node i and node j. If a dual porosity - dual permeability system is modelled, then η_i contains the geometric neighbours as in the single porosity case, as well as the matrix/fracture node which is physically considered to be in the same location. Because of the random nature of fractured rock, it is possible to account for the matrix-fracture coupling only in an average way. For example, the product

$$\gamma_{ij} \; K_{j+\frac{1}{2}} \tag{8}$$

can be approximated by:

$$4 V_i \left[\frac{1}{L_x^2} + \frac{1}{L_y^2} + \frac{1}{L_z^2} \right] K_{\text{matrix}} \tag{9}$$

where L_x, L_y, L_z are the average fracture spacings in the directions x, y, and z [11].

Consequently, modelling a dual porosity system with N finite volumes results in $2N$ nodes. The convention that nodes $(1-N)$ represent matrix nodes, while nodes $(N+1, \ldots, 2N)$ represent fracture nodes was used in this work.

It is interesting to observe that a dual porosity system of physical dimensionality d has similar characteristics to a single porosity system of dimension $d+1$, in terms of connectivity and magnitude of computational work. In fact, as has been discussed

previously [11], any $3-d$ single porosity code can be used to solve $2-d$ dual porosity problems.

The subscript (jup) in equations (4-6) indicates upstream weighting, while $(j+\frac{1}{2})$ indicates harmonic average [17] for absolute permeability, heat conductivity, and diffusion coefficient terms. The upstream direction is determined by the sign of the appropriate phase potential gradient.

4. Primary Variable Substitution

Equations (4-6) are fully implicit, and consequently give rise to a large system of non-linear algebraic equations. This system of equations is solved using full Newton iteration. For each node, three primary variables are selected. The primary variables are regarded as independent variables when constructing the Jacobian. Any other quantitites defined at node i in equations (4-6) are dependent on the primary variables for that node. The Newton iteration increments for the primary variables are given from the solution of the Jacobian system.

For any node where both liquid and gas phases are present, the primary variables are selected to be:

$$P_g\,,\ S_\ell\,,\ T \tag{10}$$

with:

$$P_\ell = P_g - P_{cg}(S_\ell) \tag{11}$$

$$S_g = 1 - S_\ell$$

where $P_{cg}(S_\ell)$ is the capillary pressure. Phase equilibrium between liquid and gas phases is assumed to be of the form:

$$Y_a = Z_a(P_g\,,\ T)X_a \tag{12}$$

$$Y_w = Z_w(P_g\,,\ P_{cg}\,,\ T)X_w$$

along with the constraints:

$$X_a + X_w = 1 \tag{13}$$

$$Y_a + Y_w = 1$$

Given the set of primary variables $(P_g\,,\ S_\ell\,,\ T)$, then equations (12-13) represent a phase equilibrium or flash calculation which can be solved for $(X_a\,,\ Y_a\,,\ X_w\,,\ Y_w)$.

If, after any Newton iteration,

$$S_{\ell i} < 0$$

then this indicates that the liquid phase has disappeared (due to boiling in node i) and that superheated steam is present. When this occurs, the primary variables in node i are switched to:

$$P_g\,,\ T\,,\ Y_a \tag{13}$$

with the constraints:

$$\begin{aligned} S_\ell &= 0 \\ Y_g &= 1 - Y_a \\ X_a &= \frac{Y_a}{Z_a} \\ X_w &= \frac{Y_w}{Z_w}\,. \end{aligned} \tag{14}$$

When a node is in this (superheated) state, the quantity:

$$X_a + X_w$$

is monitored. If this quantity becomes larger than one, then this indicates that the liquid phase has appeared (due to condensation), and so the primary variables are switched back to $(P_g\,,\ S_\ell\,,\ T)$ with the constraints (11-13).

If a cell is in the two phase state (equation (10)), and any Newton iteration produces a cell with:

$$S_g < 0 \tag{15}$$

then the primary variables in this cell are switched to:

$$P_g\,,\ T\,,\ X_a \tag{16}$$

with the constraints:

$$\begin{aligned} S_g &= 0 \\ Y_a &= Z_a\, X_a \\ X_w &= 1 - X_a \end{aligned} \tag{17}$$

$$Y_w = Z_w X_w .$$

When a cell is in this state (single phase liquid), the quantity:

$$Y_a + Y_w$$

is monitored. If this quantity becomes larger than one, then this cell is switched to the two phase state.

The above variable substitution method handles all possible cases of phase appearance/disappearance. Of course, Z_a is normally very large, so that any amount of air appearing in a cell with $S_g = 0$ will trigger the appearance of the gas phase. However, if we had used the reasonable approximation that X_a is identically zero, then the two phase primary variable set (P_g, S_ℓ, T) would have to be used in the event that no gas phase was present. This is because even if $S_g = 0$ in node i, gas could appear due to convection from a neighbouring node at any time. In any situation where:

$$\begin{aligned} &|S_g| < \epsilon \\ &|Y_a| < \epsilon \\ &|\epsilon| << 1 \end{aligned} \tag{19}$$

in node i, and Δt is small, then the line of the Jacobian corresponding to the air conservation equation in cell i would be nearly zero, and the Jacobian nearly singular. This, of course, would cause difficulties for the Newton iteration, and can cause convergence to non-physical solutions [18]. The inclusion of non-zero (although small) X_a avoids these difficulties, since there is always a suitable test for appearance/disappearance of any phase. In particular, consider a two phase state where the conditions described in equation (19) occur. Equation (4) has large derivatives with respect to P_g and T, since X_a is a strong function of these quantities due to equations (12-13).

It is possible to select a set of variables which is always meaningful, regardless of the presence or absence of phases. However, physical properties have drastically different values depending on the absence or presence of a phase. For example, the compressibility of a single phase liquid system is much smaller than a two phase liquid-steam system, even if the amount of steam is very small. Consequently, if a single set of variables is used, some difficulties will be enountered in attempting to calculate meaningful derivatives when phase appearance/disappearance is occuring.

Since complex physical correlations are used for the *PVT* properties (see the Appendix), the Jacobian is constructed numerically. It is important to keep a cell in the same state when shifting primary variables in the numerical derivative calculation. For example, if the numerical shift causes a saturation to go negative, the thermodynamic state of the cell is not switched. If a cell is allowed to switch during the numerical differentiation process, then convergence of the Newton iteration is very poor. This problem is difficult to avoid if the same set of primary variables is always used in conjunction with a general flash calculation for *PVT* properties.

The Jacobian matrix is solved using an incomplete *LU* factorization iterative solver with Orthomin acceleration [19-20].

5. Choice of Primary Variables

Some initial tests of the numerical scheme described in the previous sections were carried out for a comparatively easy problem similar to that described in Reference [7]. In this large scale simulation, the waste repository was modelled as a disc 1500 m in radius, with a distributed heat source of $14\,W/m^2$, which decays over time [7]. Since the heat flux is averaged out in the areal direction, the heating effect is very gentle. In fact, very little change takes place in the liquid saturation values (even near the heat sources), and the temperature never rises above $100\,^\circ$ C. The domain of the problem is shown in Figure 2, and the physical properties data is given in Table 1. The problem was modelled using a coarse 10×10 grid, with the double porosity - double permeability assumptions.

An initial prototype code used the liquid phase pressure P_ℓ as a primary variable instead of the gas phase pressure P_g as described in Section 4. Solution of this comparatively easy problem using the dual porosity approach proved to be unexpectedly difficult. Very poor convergence of the Newton iteration was observed, with a large number of repeat timesteps.

Since the rock capillary pressure was very large (approximately $10^4\,Kpa$ at $S_\ell = .9$), any liquid phase appearing in the fractures was immediately withdrawn into the nearest matrix cell. Consequently, the converged liquid saturation in the fractures was essentially zero throughout the course of the simulation. (Recall that the critical liquid saturation in the fractures is zero, viz. Table 1). Problems were observed whenever a saturated gas at high temperature flowed into a region of cooler temperatures. The first Newton iteration would cause liquid water to appear in the fractures (due to phase equilibria conditions), and then this water would be subject to

a large capillary pressure suction which would draw the liquid into the rock matrix. This would cause an overshoot in the Newton iterations, and oscillatory changes were produced. Liquid would appear, disappear, reappear, and so on, in the same fracture cell. This could cause extremely slow convergence. Various under-relaxation schemes were tried without success.

This would seem to be a peculiar situation, since the converged result from the previous timestep was $S_\ell = 0.0$ in the fractures. In other words, the initial guess, at least as far as S_ℓ is concerned, is close to the exact solution. However, this effect can be explained in the following qualitative way: the driving force for gas phase flow is the gas phase pressure gradient. Consequently, since the gas phase pressure is given by:

$$P_g = P_\ell + P_{cg}\,(S_\ell) \tag{20}$$

then the gas pressure gradient term has a very large derivative with respect to S_ℓ, when $(P_\ell\,,\ S_\ell\,,\ T)$ are primary variables $(S_\ell \neq 0)$. This large derivative is multiplied by the large absolute permeabilities of the fracture system, and appears in both diagonal and off-diagonal blocks of the Jacobian. Consequently, any small amount of S_ℓ appearing in a fracture node can cause very large changes to be predicted by the Newton iteration, and hence an oscillation is set up. If, on the other hand, P_g is selected as the independent variable, then there is no derivative with respect to S_ℓ in the gas phase pressure gradient term. A large derivative does appear in the liquid phase pressure gradient since:

$$P_\ell = P_g - P_{cg}\,(S_\ell) \tag{21}$$

However, this entry in the Jacobian is small, since it is either multiplied by the relative permeability of the liquid $(K_{r\ell})$ in the fractures, or the absolute permeability of the rock matrix, both of which are small.

In order to test this hypothesis, two runs of the large scale repository model were carried out. One run used P_ℓ as the primary variable, the other run used P_g as the primary variable. The total number of Newton iterations required to reach a stopping time of ten years is reported in Table 2. The computed results at the end of ten years were virtually identical. The number of Newton iterations for the run with P_ℓ as the primary pressure variable was an order of magnitude greater than for the run with P_g as the primary pressure variable.

As a result of these tests, it was decided to switch to the variable set with P_g as the primary pressure variable. All results reported in the rest of this paper use the variable set described in Section 3.

Detailed examination of the Newton iterations with P_g as the primary pressure variable showed that the "liquid on - liquid off" oscillation was absent from these runs. If the liquid phase did appear during the course of the Newton iterations, it disappeared in the next iteration, and S_ℓ remained zero for the rest of the timestep.

Consequently, it would appear that the choice of the primary variable set can have a profound effect on the convergence characteristics for Newton iteration. It is clearly worthwhile investigating the optimum choice for any given class of problems.

6. One Dimensional Laboratory Sand Pack

In order to compare with previously obtained results, the one dimensional problem posed by Pruess was solved [8]. This example models the heat pipe which develops near a cylindrical waste package container. Pruess [8] modelled this problem using both semi-analytic and fully numerical methods. Since the heating effects are large, dry-out occurs near the canister, with the large capillary pressure providing a cool liquid feed in the two phase heat pipe region. Consequently, this example provides a good test of the numerical scheme used to solve a problem with phase disappearance and high heat flux.

The domain for this example is shown in Figure 3. One dimensional, radial co-ordinates are used, and gravity effects are neglected. The physical properties for this problem are given in Table 3.

The waste package is considered to be a cylindrical tube .2m in radius, emitting a heat flux of 500 w/m. The relative permeability and capillary pressure curves are characteristic of laboratory sand packs [8]. For this sand pack example, a single porosity model is assumed. Some of the data in Table 3 was converted from reference [8] to fit the form of the correlations used in this work (see the Appendix). This results in some unusual values for some constants (i.e. the heat conductivity of water). The air phase diffusivity was set to zero for this run.

This problem was discretized using 50 cells, as described elsewhere [8]. A steady state solution was obtained at 15 years. Plots of temperature, water saturation, and air mole fraction versus radial distance (at 15 years) are shown in Figures 4-6. The three characteristic zones are easily seen from these figures: the inner conduction zone ($S_\ell = 0$, rapid decrease in temperature), the two phase heat pipe zone (almost

constant temperature), and the outer conduction zone.

These plots are in good agreement with the numerical results presented by Pruess [8]. The numerical results in Reference [8] were also in good agreement with a semi-analytic solution.

Using the semi-analytic approximation, the peak temperature at the canister surface was predicted as 225 °C [8]. Unfortunately, the peak temperature is not given for the full numerical computation. Our result for the peak temperature is 243 °C, which, considering the various approximations involved in the semi-analytic solution, must be regarded as reasonable agreement. Further calculations by Pruess [8] with finer grids do not show any significant changes due to spatial discretization error.

The run statistics for the simulation to steady state (15 years) are given in Table 4, along with equivalent data from Pruess [8]. Although, it is generally dangerous to compare numerical results quoted on different machines, it is probably safe to assume that a CRAY-XMP is more than three times faster than a SUN 3/160. Consequently, it would appear that the numerical techniques used in this work are at least as efficient as those used previously

The average number of Newton iterations/timestep for this run was approximately 5, indicating that the non-linearities were quite severe. Note also that the air has been completely purged from the inner conduction zone and the heat pipe zone (Figure 6).

7. One Dimensional Fractured Rock Example

A leading contender for a nuclear waste disposal site in Nevada consists of highly fractured rock [21]. Consequently, realistic models of waste canister heat and mass transfer include the effect of fractures.

Typical physical data for fractured tuff formations are given in Table 5, and are similar to data used previously [10]. However, there is a high degree of uncertainty in such data as capillary pressure curves, relative permeabilities, fracture spacings, and so on. Consequently, the numerical results presented in the following must be regarded as conceptual studies.

The geometry of the problem is as shown in Figure 3, except that in this case, the outer boundary r_b was set at 59 m. Other discretization data are given in Table 5. A double porosity - double permeability approach is used. The cell spacing in the radial direction near the canister is comparable to the assumed fracture spacing (.1 m). Thus, it would be possible to model discrete fractures near the heat source. However,

in the absence of detailed information about individual fractures, the "average" approach of the double porosity model is used throughout the domain [2].

Table 6 shows the peak temperature at the canister surface at ten years. The effect of spatial discretization error can be see in the increase in peak temperature as the grid is refined. For the finest grid, the error in the peak temperature can be estimated to be approximately 3%. Since the peak temperature is the most sensitive computed parameter to grid refinement, this is the worst case estimate of truncation error. As we are interested only in the qualitative behaviour of this system, this level of error is quite acceptable. This size of discretization error is far less than the uncertainty in the physical data. All results shown in the following use the finest grid (37 cells).

Figure 7 shows the matrix temperature as a function of radial distance. The fracture temperature is not shown since it is virtually the same as the matrix temperature. There is a small kink in the curve at approximately 14 m. From Figure 8, which shows the saturation profile, we can see that the kink corresponds to the condensation zone (the liquid saturation is larger than .8). The temperature profile here is quite different from the laboratory sand pack example (Figure 4), in that the heat pipe (isothermal) zone is virtually non-existent. Some possible explanations for this phenomenon are discussed elsewhere [8].

The primary mechanism for gas phase flow is through the fractures. This is because the matrix gas phase pressure gradients are not large enough to overcome the small matrix absolute permeability. Consequently, heat is transported away from the source by vaporization of liquid water, movement of the vapour in the fracture system, and condensation of the water and movement back into the rock matrix. The large capillary pressures will not permit any finite liquid saturation in the fracture system. As a result any condensed liquid appearing in the fracture immediately moves into the nearest rock matrix cell. The large capillary pressure also results in very high liquid pressure gradients in the rock matrix, which causes the movement of water back towards the heat sources.

Figures 9 and 10 show the matrix and fracture gas phase pressure profiles. The pressure profile is fairly flat until approximately 10 m, and then reaches a maximum followed by a minimum, and finally stabilizes. The pressure increase occurs at the edge of the dried out zone, and the minimum takes place in the condensation zone (see Figure 8). Gas phase flow is always from matrix to fracture until the condensation zone is reached, and then a flow reversal takes place with gas flow from fracture to matrix.

The pressure pulse in Figure 9 can be understood more easily if the time history of cells near the canister is followed. At first, both temperature and pressure increase near the heat source. The pressure in the fracture system always remains near atmospheric, and consequently the gas flow rate from matrix to fracture is large. However, the matrix pressure remains high since the liquid water vapourizes and occupies a large volume in the gas phase, replacing the vapour which flows into the fractures. However, once the cells near the heat source dry out, the only pressure maintenance effect is the expansion of the gas phase due to heating. This effect is not sufficient to overcome the rapid depletion of gas through the fracture system, and consequently the pressure in the matrix cells behind the drying front drops rapidly, to near equilibrium with the fracture system. Ahead of the drying front, the two phase vapourization zone maintains a high pressure. The pressure minimum at the condensation front is simply due to the effect of condensation, which produces a large volume decrease, and hence a pressure minimum.

Figure 11 shows the air mole fraction profile. Because of the large heating and gas phase convection effects, the air is purged from the dried out and vapourization zones.

This pressure pulse phenomenon cannot be observed with an effective continuum approach. This is because the fracture and gas phase pressures are equal under the effective continuum assumptions.

The pressure pulse is not a transient phenomenon, since a longer computation to 100 years shows the continued existence of the pulse, although slightly reduced in size.

8. Two Dimensional Fractured Rock Example

The one dimensional problem of the previous Section was extended to a two dimensional cylindrical geometry as shown in Figure 12. The vertical rock matrix permeability was set to one tenth of the horizontal permeability. The canister was assumed to be 5 m in length.

Two sets of capillary pressure curves were used. One set (the high-P_c case) used the same capillary pressure data as used in the one dimensional run. The second set (the low-P_c case) used the table of P_{cg} values as given in Table 1, with all P_{cg} values multiplied by one tenth. Since the existence of a heat pipe zone near the canister is enhanced by a large capillary pressure, we expect that dry-out is more likely in the low-P_c case.

Table 8 shows the effect of grid size on the peak canister temperature at ten years for the low-P_c case. Again since only qualitative behaviour is of interest, this level of discretization error (approximately 3%) is quite acceptable. All results reported in the following use the 19×22 grid.

Since the high-P_c case corresponds to the physical properties used in the one dimensional runs of the previous Section, we will first present detailed results for this case. Figure 13 shows the liquid saturation contours for the high-P_c run at ten years. For visibility purposes, the contour maps are highly distorted. The grid lines are all shown as equally spaced, when in fact a very fine grid is used near the canister. The minimum liquid saturation at the canister surface is roughly $S_\ell = .33$. This is in contrast to the one dimensional computations of Section 7, where dry out occurred. Although gravitational effects may be small, the extra area available for liquid matrix flow (from above and below the cylinder) has a profound influence on the results. Clearly, one dimensional analysis of this problem can be quite misleading (i.e. it cannot be assumed that the cylinder is infinitely long).

The matrix pressure contours are shown in Figure 14 (high-P_c case). The maximum pressure is approximately 575 *Kpa*. The two lobed pressure contour (550 *Kpa*) occurs because of the complicated vapour pressure lowering effects which increase as the liquid saturation decreases [6], (see the Appendix). This results in a slightly lower pressure at cells where the liquid saturation is smallest.

Figure 15 shows the temperature contours for this case. The maximum temperature is approximately 167 °C. Note that normally we would expect the peak temperature to be much lower if a two phase zone exists near the canister. However, the high matrix pressure, and the vapour pressure lowering, inhibits the transfer of heat by latent heat of vapourization. The fracture pressure contours are not shown since the pressure in the fracture system remains very close to 100 *Kpa* for the duration of the simulation.

To enhance the possibility of dry out, the capillary pressure was reduced by a factor of ten. It is not unrealistic to examine this case since there is tremendous uncertainty in the rock matrix capillary pressures. The water saturation contours for the low-P_c are shown in Figure 16. A large dried-out zone appears near the canister. There are also two .85 contour lobes above and below the canister corresponding to condensation zones.

The matrix pressure contours are given in Figure 17. The pressure at the canister surface is roughly 100 *Kpa*, while the local maxima (approximately 300 *Kpa*) can be clearly seen. The local maxima are a two dimensional realization of the phenomena described in Section 7, with the pressure pulse appearing between the dried-out zone and the condensation zone. There is also a very slight pressure minimum in the lower condensation zone, which accounts for the two 100 *Kpa* contours.

The temperature contours in Figure 18 are surprisingly similar to the high-P_c contours in Figure 15. For this choice of physical parameters, it would appear that the heat pipe effect is not very efficient at keeping temperatures low in a fractured rock system.

Finally, Figure 19 shows the air mole fraction contours. The minimum value of the air mole fraction is approximately 7% near the canister. Although air is being purged from the vicinity of the canister, the air mole fraction never becomes zero, as for the one dimensional case.

9. Conclusions

Modelling of nuclear waste disposal in unsaturated, fractured rock requires an efficient technique for simulating phase disapparance/appearance. Phases may appear or disappear due to rapid heating effects and the large capillary pressures characteristic of fractured rock. Variable substitution was used in this work to provide a method for passing from single phase to two phase regimes and vice versa. Howover, the choice of primary variables had a marked influence on the number of Newton iterations required to solve the discretized equations. This manifested itself by a large number of phase appearance/disappearance switches. This problem was eliminated when the gas phase pressure P_g was used as part of the primary variable set instead of the liquid phase pressure P_ℓ. Consequently, special care should be taken in devising a primary variable set for these types of problems.

Numerical results were presented for a one dimensional single porosity system, which agreed with the results obtained previously using full numerical and semi-analytic methods. It would appear that the numerical techniques used here are as at least as efficient as those used previously (in the case of single porosity systems).

The dual porosity - dual permeability computations for a one dimensional system demonstrated an interesting phenomenon, which, to the best of our knowledge, has not been reported previously. A pressure pulse is observed ahead of the dried out zone near the waste canister. This pulse cannot be observed with an effective continuum

approach, since matrix and fracture gas phase pressures are assumed equal under effective continuum assumptions.

Extension of the one dimensional model to two dimensions also yielded some interesting results. In particular, the same physical parameters which gave rise to a dried out zone near the canister in one dimension did not produce a dried out zone in two dimensions. This occurred in spite of the assumption that vertical matrix permeability was one tenth the horizonal for the two dimensional computation. This was a result of the large area open for cooling water to flow back to the canister under the action of capillary pressure. In this case the two phase heat pipe zone extended all the way to the waste package. This indicates that the one dimensional calculations can be completely misleading. The usual rationale for ignoring two dimensional effects is that gravity forces are small. This may be true, but a major effect is the large geometric area factors, which are a result of the canister's finite length.

If the matrix capillary pressure was reduced by a factor of ten, a dried out zone evolved near the waste package in two dimensions. Similar to the one dimensional example, a pressure pulse (pressure maximum) was observed just ahead of the dried out zone.

Rather surprisingly, the peak canister temperature in two dimensions is roughly the same for the computations where a dried out zone occurs, and for the simulation where a two phase zone persists near the canister. This is due to the fact that the vapour pressure lowering reduces the effectiveness of the heat pipe zone.

Another effect of dimensionality may be observed in the air mole fraction profile. In one dimension, air is completely purged from the waste package environment. In two dimensions, air mole fractions of approximately 5% persist near the canister. This could have an effect on the rate of corrosion of the canister.

In summary, from the numerical point of view, variable substitution must be paired with an appropriate choice of primary variables to produce an efficient method for phase appearance/disappearance. The correct choice for the primary variable set produces a method which works well even in the case of large matrix capillary pressures. It is clearly important to carry out multi-dimensional, dual porosity calculations to produce accurate predictions of the waste canister environment. One dimensional, effective continuum approaches are incapable of simulating all the important physical processes.

References

[1] M. Stanish, G. Schajer, F. Kaythan, *"A Mathematical Model of Drying for Hygroscopic Porous Media,"* AICLE Journal *32* (1986) 1301-1311.

[2] K. Pruess, *"Heat Transfer in Fractured Geothermal Reservoirs with Boiling,"* Water Res. Res. *19* (1983) 201-208.

[3] T. Chawla, D. Pederson, W. Minkowycz, *"Governing Equations for Heat and Mass Transfer in Heat-generating Porous Beds - I. Coolant Boiling and Transient Void Propagation,"* Int. J. Heat Mass Transfer *28* (1985) 2129-2136.

[4] B. Travis, S. Hodison, H. Nuttal, T. Cook, P. Rundberg, *"Numerical Simulation of Flow and Transport in Fractured Tuff,"* Mat. Rec. Soc. Symp. Proc. *26* (1984) 1039-1046.

[5] K. Pruess, J. Wang, *"Tough-A Numerical Model for Nonisothermal Unsaturated Flow to Study Waste Canister Heating Effects"*, Mat. Rec. Soc. Symp. Proc. *26* (1984) 1031-1038.

[6] D.W. Pollock, *"Simulation of Fluid Flow and Energy Transport Processes Associated with High-Level Radioactive Water Disposal in Unsaturated Alluvium,"* Water Res. Res. *22* (1986) 765-775.

[7] Y. Tsang and K. Pruess, *"A Study of Thermally Induced Convection Near a High Level Nuclear Waste Repository in a Partially Saturated Fractured Tuff,"* Water Res. Res. *23* (1983) 1958-1966.

[8] C. Doughty, K. Pruess, *"A Semianalytical Solution for Heat-Pipe Effects Near High-Level Nuclear Waste Packages Buried in Partially Saturated Geological Media,"* Int. J. Heat Mass Transfer *33* (1988) 79-90.

[9] K. Udell, *"Heat Transfer in Porous Media Considering Phase Change and Capillarity - the Heat Pipe Effect,"* Int. J. Heat Mass Transfer *28* (1985) 485-495.

[10] K. Pruess, Y. Tsang, J. Wang, *"Modelling of Strongly Heat Driven Flow in Partially Saturated Fractured Porous Media,"* in Proceedings IAH 17th Int. Cong. on Hydrogeology of Rocks of Low Permeability, Tucson, 1985.

[11] R. Dean, L. Lo, *"Simulation of Naturally Fractured Reservoirs," Soc. Pet. Eng. J. Res. Eng. 3* (1988) 638-648.

[12] J. Gillman, H. Kazemi, *"Improvements in Simulation of Naturally Fractured Reservoirs,"* Soc. Pet. Eng. J. *23* (1983) 695-707.

[13] K. Pruess, T. Narasimham, *"A Practical Method for Modelling Heat Flow in Fractured Porous Media,"* Soc. Pet. Eng. J. *25* (1985) 14-26.

[14] C. Prakash, *"Examination of the Upwind Formulation in the Control Volume Finite-Element Method for Fluid Flow and Heat Transfer,"* Num. Heat Trans. *11* (1987) 401-416.

[15] R. Bank, D. Rose, *"Some Error Estimates for the Box Method,"* SIAM J. Num. Anal. *24* (1987) 777-787.

[16] P.A. Forsyth, *"A Control Volume Finite Element Method for Local Mesh Refinement," Proc. 10th SPE Symposium on Reservoir Simulation, Houston, 1989.*

[17] K. Aziz, A. Settari, *"Petroleum Reservoir Simulation,"* Applied Science, London, 1979.

[18] P.A. Forsyth, B. Rubin, P. Vinsome, *"The Elimination of the Constraint Equation and Modelling of Problems with a Non-Condensable Gas in Steam Simulation,"* J. Cdn. Pet. Tech. Oct.-Dec. (1981) 63-69.

[19] A. Behie, P.A. Forsyth, *"Incomplete Factorization Methods for Fully Implicit Simulation of Enhances Oil Recovery,"* SIAM J. Sci. Stat. Comp. *5* (1984) 543-561.

[20] P.A. Forsyth, P.H. Sammon, *"Practical Consideration for Adaptive Implicit Methods in Reservoir Simulation,"* J. Comp. Phys. *62* (1986) 265-281.

[21] J. Wang, T. Narasimham, *"Hydrologic Mechanisms Governing Fluid Flow in a Partially Saturated, Fractured, Porous Medium,"* Water Res. Res. *21* (1985) 1861-1874.

Table 1

Physical data for problems 1 and 3. Other data and correlations are given in the Appendix.

Rock Matrix

Permeability	$1.9 \times 10^{-18}\ m^2$
Porosity	.11
Heat capacity of rock	$2.35 \times 10^6\ J/(m^3 - {}^\circ K)$
Compressibility of Rock (C_R)	$1.5 \times 10^5\ J/(m - {}^\circ K - \text{day})$

Fractures

Permeability	$1.8 \times 10^{-14}\ m^2$
Porosity	.0018
Spacing $(L_x = L_y = L_z)$	$.1m$

Table 1(a)

Fluid properties

Heat conductivity of liquid	5.35×10^4 $J/(m - {}^\circ K - \text{day})$
Heat conductivity of air	$.26 \times 10^4$ $J/(m - {}^\circ K - \text{day})$
Heat conductivity of rock	1.5×10^5 $J/(m - {}^\circ K - \text{day})$
Diffusion constant for the gas phase, D_g^0 (see the Appendix)	$.41 \times 10^5$ m^2/sec

Table 1(b)

Relative permeability and capillary pressure for the rock matrix.

S_ℓ	$K_{r\ell}$	K_{rg}	$P_{cg}\ (Kpa)$
0.0	0.0	1.0	4.8×10^{6}
0.1	2×10^{-6}	1.0	2.9×10^{5}
0.2	7×10^{-5}	1.0	1.2×10^{5}
0.3	5.5×10^{-4}	1.0	7.2×10^{4}
0.4	2.4×10^{-3}	1.0	4.9×10^{4}
0.5	7.5×10^{-3}	.99	3.5×10^{4}
0.6	.02	.98	2.6×10^{4}
0.7	.047	.95	1.9×10^{4}
0.8	.11	.89	1.3×10^{4}
0.9	.24	.76	8.3×10^{3}
1.0	1.0	0.0	0.0

Table 1(c)

Relative permeability and capillary pressure for the fracture

$$K_{r\ell} = S_\ell$$
$$K_{rg} = 1 - S_\ell$$
$$P_{cg} = 0.0 \quad \forall \; S_\ell$$

Initital conditions

Rock Matrix	**Fractures**
$T = 26\,^\circ C$	$T = 26\,^\circ C$
$P_g = 100\ Kpa$	$P_g = 100\ Kpa$
$S_\ell = 0.9$	$S_\ell = 0.0$

Boundary conditions

$T = 26\,^\circ C$, $P_g = 100\ Kpa$ at surface

$T = 26\,^\circ C$ on bottom

No-flow on all other edges.

Table 2

Total number of Newton iterations for the large scale simulation, stopping time 10 years.

Primary Pressure Variable	Total Newton Iterations
P_g	52
P_ℓ	562

Table 3

Physical properties for the one dimensional laboratory sand pack example. Only those properties which are different from Table 1 are listed below. Other correlations and data are in the Appendix.

Rock Matrix

Permeability	$10^{-12}\ m^2$
Porosity	0.4
Heat capacity of rock	$2.35\times10^{6}\ J/(m^3-^\circ K)$
Compressibility of rock (C_R)	$5.0\times10^{-6}\ (Kpa)^{-1}$
Heat conductivity of rock	$8.3\times10^{4}\ J/(m-^\circ K-\text{day})$

Table 3(a)

Fluid properties

Heat conductivity of water	1.3×10^5 $J/(m - {}^\circ K - \text{day})$
Heat conductivity of air	6.5×10^3 $J/(m - {}^\circ K - \text{day})$
Diffusion constant for air	0.0

Relative permeability and capillary pressure

$$S^* = (S_\ell - .15)/.85$$

$$K_{r\ell} = (S^*)^3$$

$$K_{rg} = (1 - S^*)^3$$

$$P_{cg} = 36.0\,(\,a\,(1 - S^*) + b\,(1 - S^*)^2 + c\,(1 - S^*)^3) \quad Kpa$$

$a = 1.417 \quad b = 1.12 \quad c = 1.263$

Table 3(b)

Initial conditions

$T = 26\,^{\circ}C$
$P_g = 100\ Kpa$
$S_\ell = 0.8$

Boundary conditions

At	$r_b = 10m$	$P_g = 100\ Kpa$
		$T = 26\,^{\circ}C$
		$S_\ell = 0.8$
At	$r_c = 0.2m$	Heat source of
		$500\ W/m$

Discretization data

$\triangle r = 0.2m$	$0.0 - 0.2m$
$\triangle r = 0.1m$	$0.2 - 4.0m$
$\triangle r = 0.6m$	$4.0 - 10.0m$

Table 4

Run statistics for the one dimensional laboratory sand pack problem. The steady state is reached at 15 years.

	This work	Previous work [8]
Timesteps	95	300
CPU time	8.2 min (SUN 3/160)	2.7 min (CRAY-XMP)

Table 5

Data for one dimensional fractured rock example. All physical properties as given in Table 1, other correlations in the Appendix.

Discretization Data

One dimensional radial co-ordinates. For the grid with 10 cells:

$$\triangle r = .2, .1, .2, .4, .8, 1.6, 3.2, 7.5, 15.0, 30.0\, m$$

For the 19 cell grid:

All the above $\triangle r$ halved, except for the first cell.

For the 37 cell grid:

All the above $\triangle r$ halved again, except for the first cell.

Table 5(a)

Initial conditions

Rock Matrix	**Fractures**
$T = 26\,^{\circ}C$	$T = 26\,^{\circ}C$
$P_g = 100\ Kpa$	$P_g = 100\ Kpa$
$S_\ell = 0.8$	$S_\ell = 0.0$

Boundary conditions (see Figure 3)

At	$r_b = 30\,m$	$p_g = 100\ Kpa$ $T = 26\,^{\circ}C$
At	$r_c = 0.2\,m$	Heat source of 500 W/m

Table 6

Peak temperature at the canister surface for the one dimensional fractured rock example, for various grid sizes.

Number of cells	Peak Temperature ($^\circ C$)
10	225
19	235
37	242

Table 7

Data for two dimensional fractured rock example. All physical properties as given in Table 1, other correlations given in the Appendix. Vertical matrix permeability is one tenth horizontal matrix permeability.

Discretization Data (cylindrical co-ordinates)

10×11 grid

$$\triangle r = .2, .1, .2, 4, .8, 1.6, 3.2, 7.5, 15.0, 30.0\, m$$

$$\triangle z = 8.0, 4.0, 2.0, 1.0, 1.0, 1.0, 1.0, 1.0, 2.0, 4.0, 8.0$$

All cells halved for the 19×22 grid

Initial Conditions

Rock Matrix	**Fracture**
$T = 26\,^{\circ} C$	$T = 20\,^{\circ} C$
$P_g = 100\, Kpa$	$P_g = 100\, Kpa$
$S_\ell = 0.8$	$S_\ell = 0.0$

Table 7(a)

Boundary Conditions:

At $r = 0.2\,m$, depth $= 14\,m$ *to* $19\,m$, heat source of $500W/m$

At $r = 59\,m$, depth $= 0$ *to* $33\,m$

$P_g = 100\,Kpa$, $T = 26\,^{\circ}C$

At depth $= 0.0\,m$, $r = 0.0 - 59\,m$,

$T = 26\,^{\circ}C$, no fluid flow

At depth $= 33\,m$, $r = 0 - 59\,m$,

$T = 26\,^{\circ}C$, no fluid flow

Table 8

Comparison of peak temperatures at the canister surface, for the two dimensional, *Low-*P_c runs, different grid sizes.

Grid Size	**Peak Temperature** ($^\circ C$)
10×11	171.3
19×22	176.2

Nomenclature

A_{ij}	-	interfacial area between cell i and cell j $[m^2]$
C_R	-	compressibility of rock $[Kpa^{-1}]$
D	-	depth $[m]$
D_g	-	gas phase diffusion constant $[m^2/\text{day}]$
g	-	acceleration due to gravity $[Km/\text{sec}^2]$
h_m	-	enthalpy of phase m $[j/\text{mole}]$
h_{lat}	-	latent heat of vaporization $[J/\text{mole}]$
K	-	absolute permeability $[m^2]$
K_{rm}	-	relative permeability
L_x , L_y , L_z	-	fracture spacing in x, y, z directions $[m]$
M_m	-	molar density of phase m $[\text{mole}/m^3]$
P_m	-	pressure of phase m $[Kpa]$
P_{cg}	-	liquid-gas capillary pressure $[Kpa]$
$q_m{}'$	-	source/sink term of phase m $[m^3/\text{day}]$
$q_{en}{}'$	-	source/sink term for energy $[J/\text{day}]$
R	-	ideal gas constant $[Kpa - m^3/(\text{mol}-^\circ K)]$
r_c	-	canister radius $[m]$
r_b	-	outer domain boundary radius $[m]$
S_m	-	saturation of phase m
T	-	temperature $[^\circ K]$
U_m	-	internal energy of phase m $[J/\text{mole}]$
V_i	-	volume of i^{th} finite volume
W_p	-	molecular weight of component p $[Kg/\text{mole}]$
X_p	-	mole fraction of component p in the liquid phase
Y_p	-	mole fraction of component p in the gas phase
Z_p	-	equilibrium ratio (Y_p/X_p) for component p
α_m	-	coefficient in molar density formula $[Kpa^{-1}]$
β_m	-	coefficient in molar density formula $[^\circ K^{-1}]$
γ_{ij}	-	geometric factor in finite volume of discretization $[m]$
Δr	-	size of finite volume in radial direction $[m]$
Δx_{ij}	-	distance between node i and node j $[m]$

$\triangle t$	-	timestep size
ϕ	-	porosity
λ	-	effective heat conductivity of rock and fluids $[J/(m-\text{day}-^{\circ}K)]$
η_i	-	neighbour set of node i
μ_m	-	viscosity of phase m $[Kpa-\text{day}]$

Appendix

This Appendix gives some of the correlations used for various physical properties. Any data given below were used for all the examples described in this work.

Molar Densities

$$M_w = M_{wr}\,[1 + \alpha_w(P_\ell - P_r) - \beta_w\,(T - T_r)] \text{ mole}/m_3$$

$$M_{wr} = 5.55 \times 10^4 \text{ mole}/m^3$$

$$\alpha_w = 4.3 \times 10^{-6}\ (Kpa)^{-1}$$

$$\beta_w = 2.1 \times 10^{-4}\ (^\circ K)^{-1}$$

$$T_r = 273\ ^\circ K$$

$$P_r = 100\ Kpa$$

$$M_g = P_g / R\,T \text{ mole}/m^3$$

$$R = 8.314 \times 10^{-3}\ Kpa\text{–}m^3/(\text{mol–}^\circ K)$$

Mass Density

$$\rho_\ell = M_w\,(W_w\,X_w + W_a\,X_a)\ Kg/m^3$$

$$\rho_g = M_g\,(W_w\,Y_w + W_a\,Y_a)\ Kg/m^3$$

$$W_w = 18.02 \times 10^{-3}\ Kg/\text{mole}$$

$$W_a = 28.97 \times 10^{-3}\ Kg/\text{mole}$$

Equilibrium ratios:

$$Y_a = Z_a X_a$$

$$Y_w = Z_w X_w$$

$$Z_a = 1 \times 10^9 / (7.6\ P_g\ \alpha^*)$$

α^* linearly interpolated from the table:

$T(^\circ K)$	α^*
273	30.5
293	19.8
323	13.9

$$Z_w = \exp\left[\frac{-P_{cg}(S_\ell)}{M_\ell\, R\, T}\right] Z_w^s$$

$P_{cg}(S)$ = capillary pressure

Z_w^s = normal equilibrium ratio (no capillary effects)

$$= \frac{.8777 \times 10^{-8} (T - 243)^{4.76}}{P_g}$$

Note the vapour pressure lowering effects (reduction of Z_w) due to capillary pressure effects [6,7].

Enthalpies:

$$h_\ell = C_w (T - T_r) X_w + C_a (T - T_r) X_a \quad J/\text{mole}$$

$$C_w = 75.4 \quad J/(\text{mole}-^\circ K)$$

$$C_a = 29.2 \quad J/(\text{mole}-^\circ K)$$

$$T_r = 273\,^\circ K$$

$$h_{ga} = C_a (T - T_r) \quad J/\text{mole}$$

$$H_{gw} = C_w (T_s - T_r) + h_{\text{lat}} + 30.5 (T - T_s) \quad J/\text{mole}$$

$$T_s = T \quad \text{if} \quad S_\ell \neq 0$$

$$= \text{solution } of \text{ equation:}$$

$$Y_w - Z_w (T_s) = 0 \quad \text{if} \quad S_\ell = 0$$

$$h_{\text{lat}} = 4.814 \times 10^3 (T_c - T_s)^{.38} \quad J/\text{mole} \quad T_s < T_c$$

$$= 0 \qquad\qquad T_s > T_c$$

$$T_c = 647.3\ ^\circ K$$

$$h_g = Y_w h_{hw} + Y_a h_{ga}$$

Internal Energies

$$U_w = h_w - \frac{P_w \times 10^3}{M_w} \quad J/\text{mole}$$

$$U_g = h_g - \frac{P_g \times 10^3}{M_g} \quad J/\text{mole}$$

units of P_w, $P_g = Kpa$

Heat capacity of rock

$$U_r M_r = 2.35 \times 10^6 \quad J/(m^3 - ^\circ K)$$

Viscosities

$$\mu_w = 10^{-9}/(12.1 + 2.88\,T^* + 7.78\times 10^{-4}(T^*)^2) \quad Kpa-\text{day}$$

$$T^* = T - 273$$

$$\mu_g = 10^{-13}(1.574 + .0044\,T^*)\ Kpa-\text{day}$$

Gas phase diffusivity [7]

$$D_g = \frac{D_g^0\,\phi\,S_g\,(T/273)^{2.334}}{(P_g/100)}$$

Heat conductivity of matrix

$$\lambda = (1-\phi)\,\lambda_{\text{rock}} + \phi\,(S_\ell\,\lambda_{\text{wat}} + S_g\,\lambda_{\text{air}})$$

See Table 1 for λ_{rock}, λ_{wat}, λ_{air}

Heat conductivity of fracture fluids

$$\lambda = \phi\,(S_\ell\,\lambda_{\text{wat}} + S_g\,\lambda_{\text{air}})$$

$$\phi = \phi_0\,[1 + C_R\,(P_e - P_r)]$$

Porosity

$$\phi = \phi_0\,[1 + C_R\ (P_e - P_r)]$$

Figure Captions

(1) Control volume containing both rock matrix and fracture cells.

(2) Domain for large scale waste repository model.

(3) Cylindrical waste package geometry.

(4) Temperature for one dimensional laboratory sand pack.

(5) Saturation profile for one dimensional laboratory sand pack.

(6) Air mole fraction for one dimensional laboratory sand pack.

(7) Rock matrix temperature, one dimensional fractured rock example.

(8) Rock matrix saturation, one dimensional fractured rock example.

(9) Rock matrix gas phase pressure, one dimensional fractured rock example.

(10) Fracture gas phase pressure, one dimensional fractured rock example.

(11) Fracture air mole fraction, one dimensional fractured rock example.

(12) Geometry for two dimensional fractured rock example.

(13) Matrix water saturation, High-P_c case.

(14) Matrix gas phase pressure, High-P_c case.

(15) Matrix temperature, fractured rock example, High-P_c case.

(16) Matrix water saturation, Low-P_c case.

(17) Matrix gas phase pressure, Low-P_c case.

(18) Matrix temperature, Low-P_c case.

(19) Matrix air mole fraction, Low-P_c case.

FIGURE 1

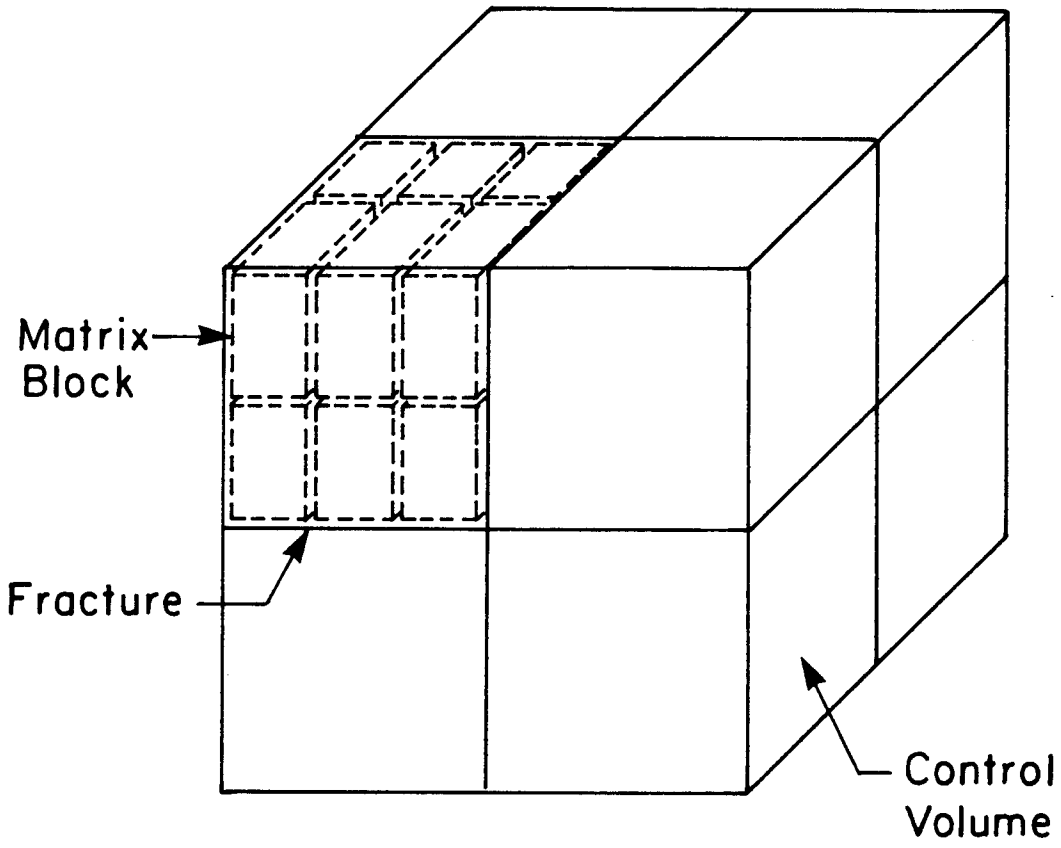

Control volume containing both rock matrix and fracture cells.

FIGURE 2

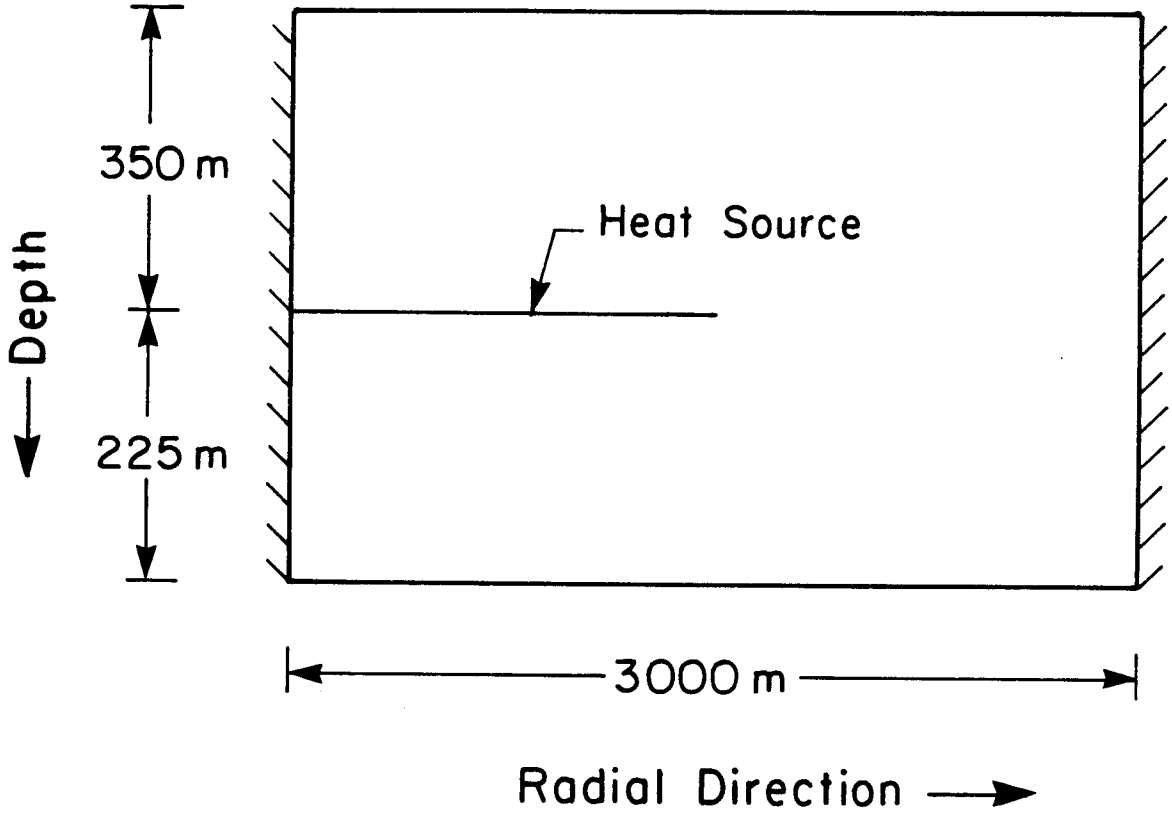

Domain for large scale waste repository model.

FIGURE 3

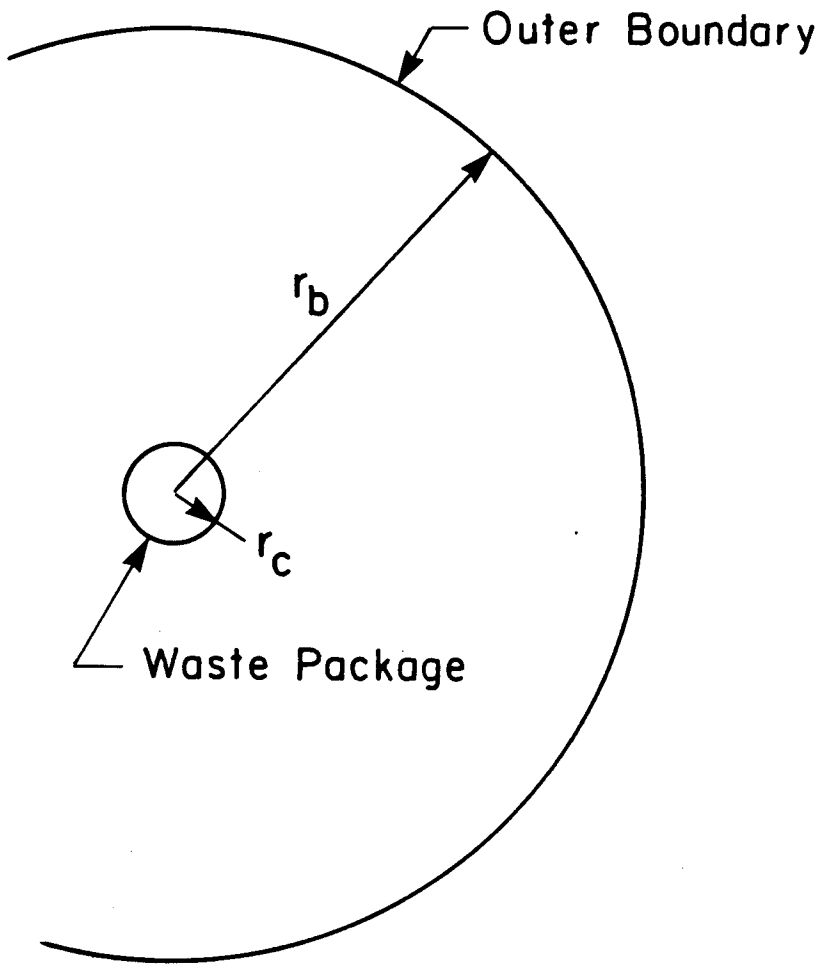

Cylindrical waste package geometry.

FIGURE 4

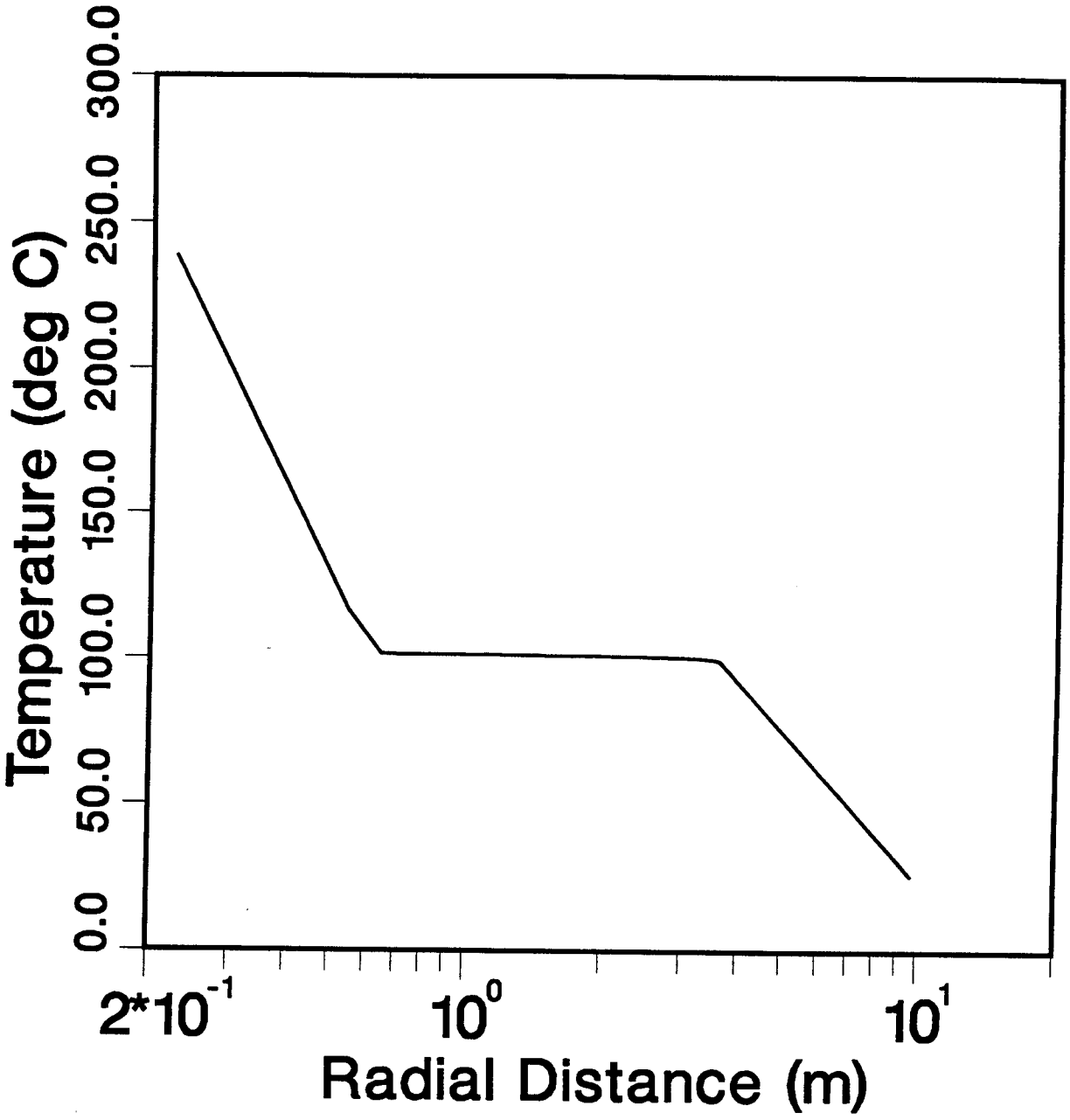

Temperature for one dimensional laboratory sand pack.

FIGURE 5

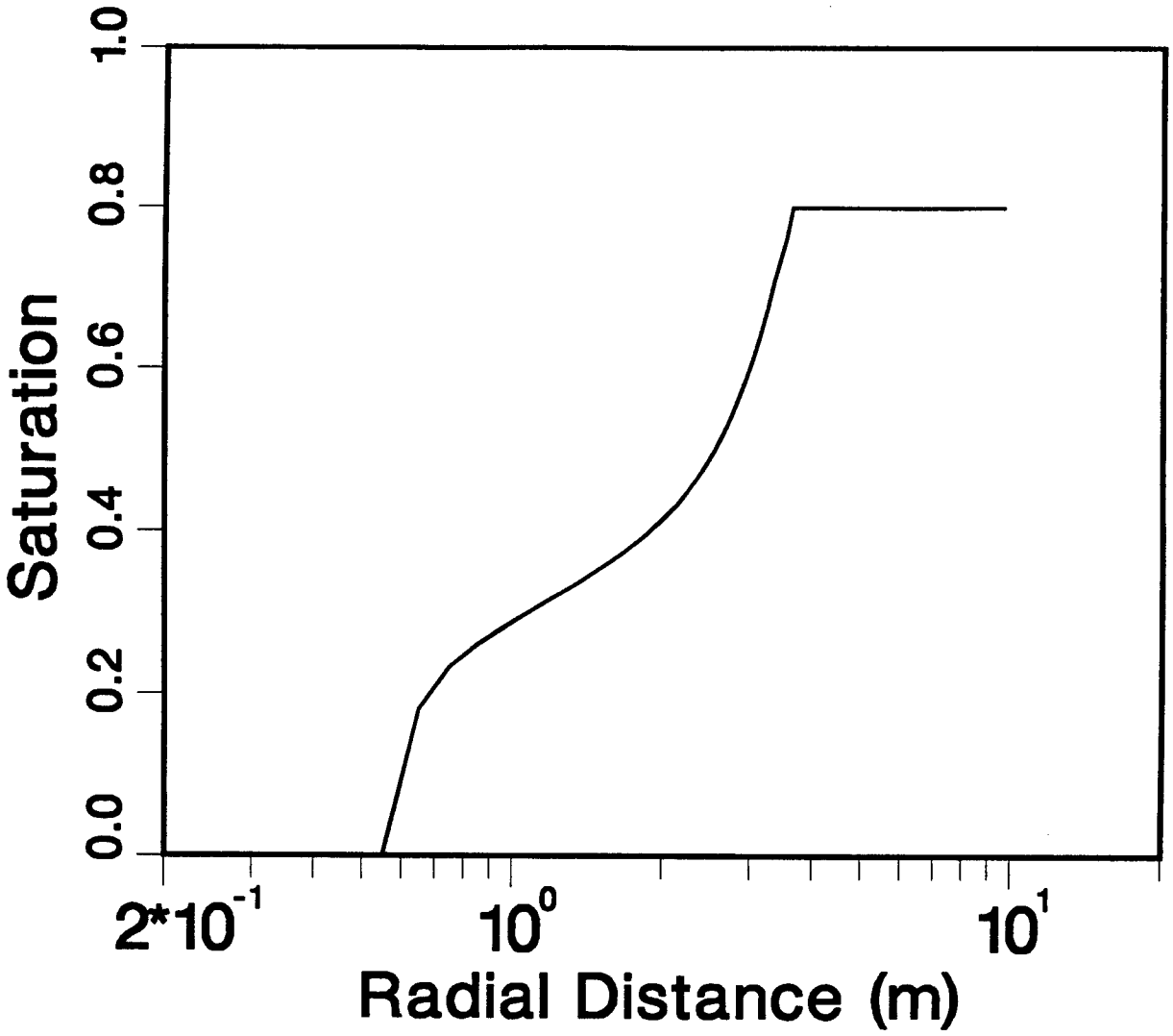

Saturation profile for one dimensional laboratory sand pack.

FIGURE 6

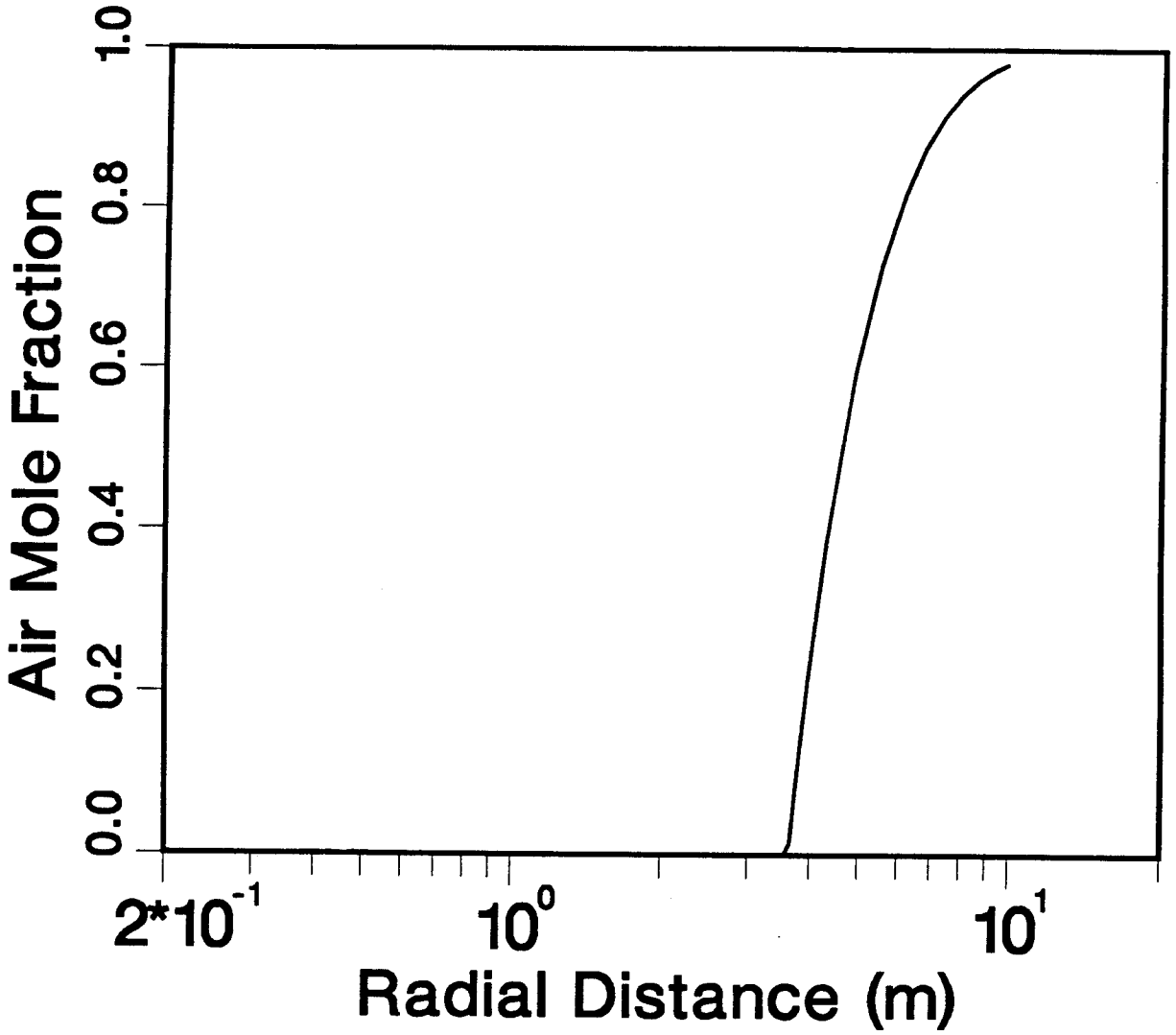

Air mole fraction for one dimensional laboratory sand pack.

FIGURE 7

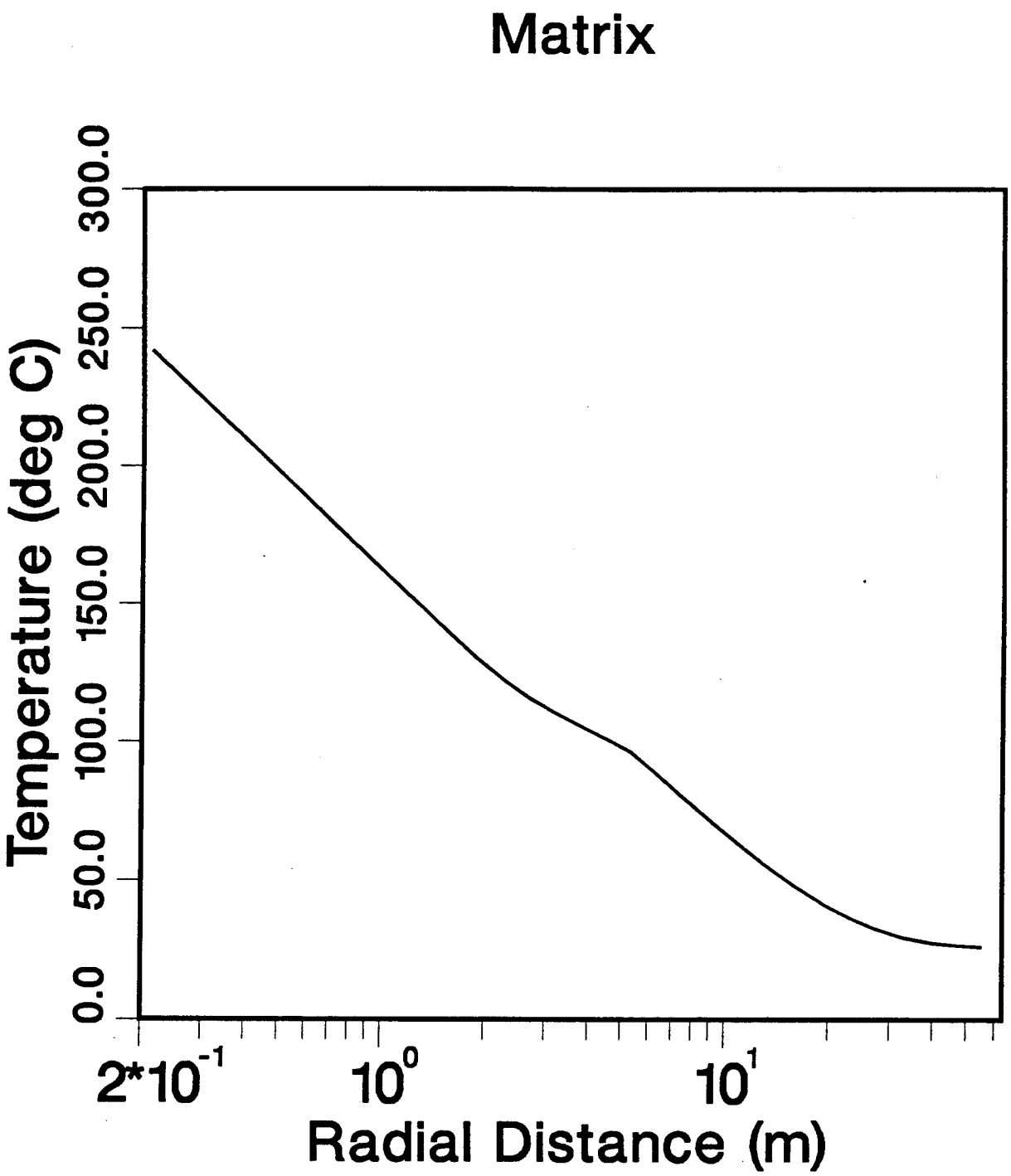

Rock matrix temperature, one dimensional fractured rock example.

FIGURE 8

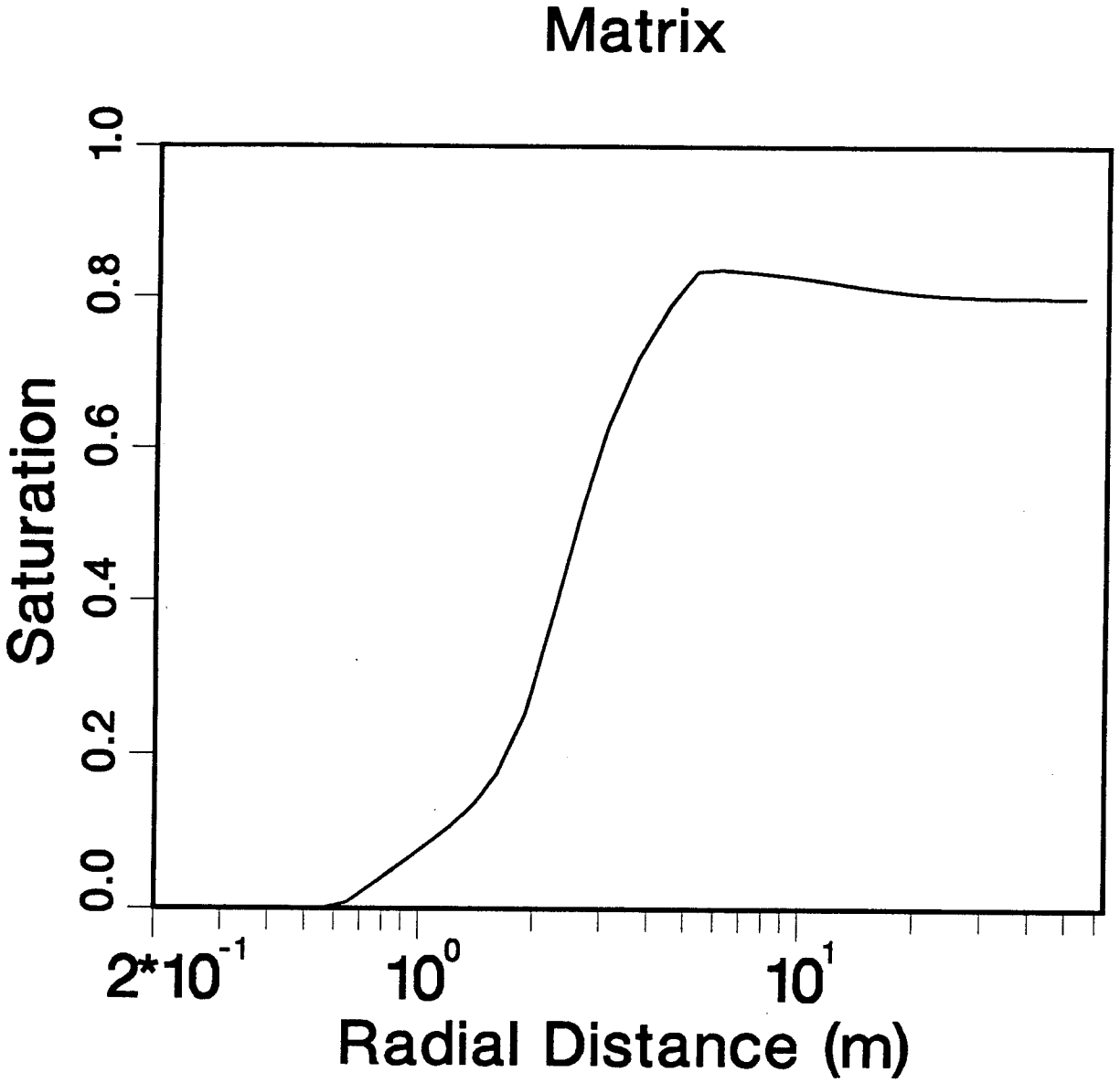

Rock matrix saturation, one dimensional fractured rock example.

FIGURE 9

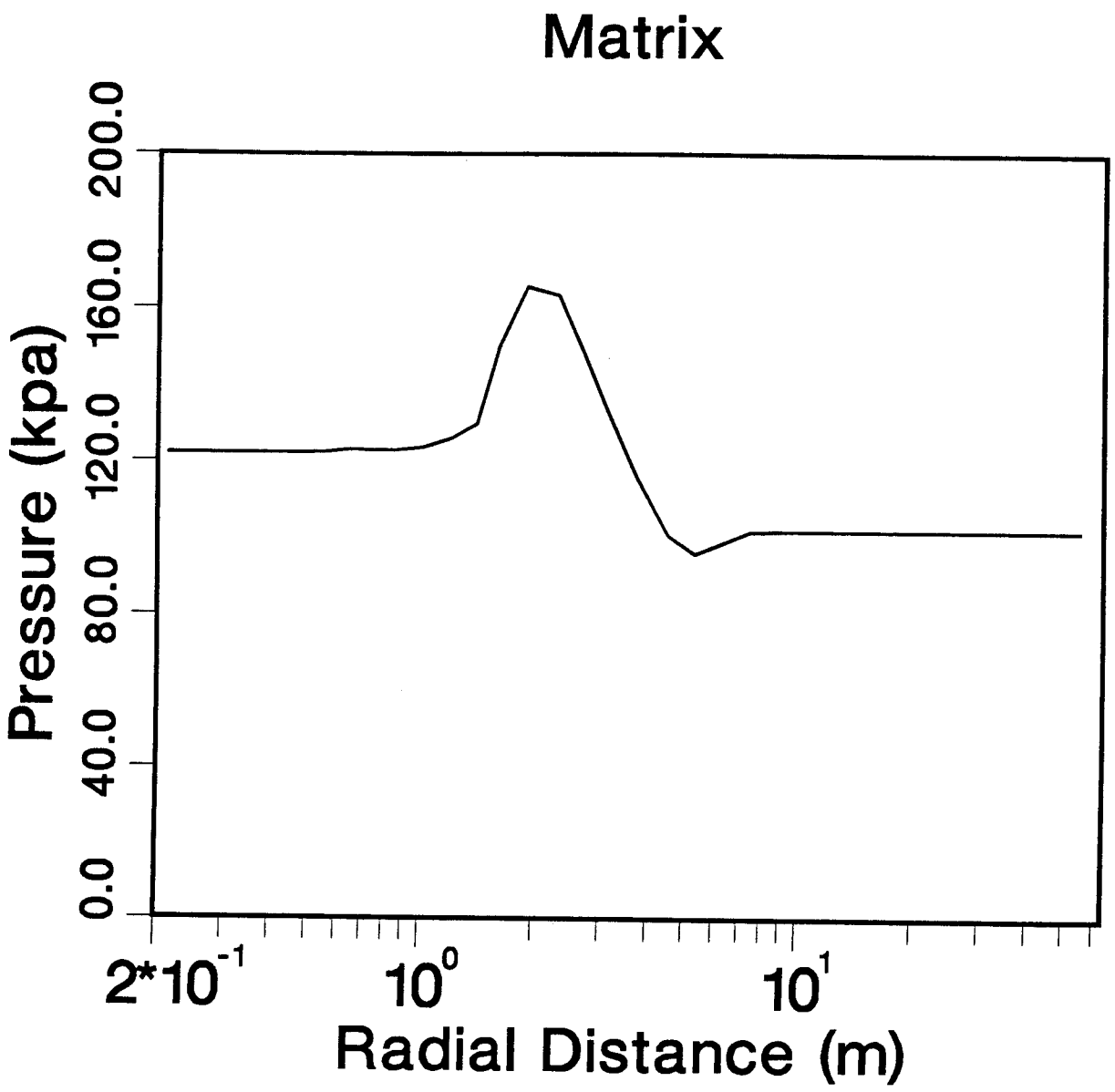

Rock matrix gas phase pressure, one dimensional fractured rock example.

FIGURE 10

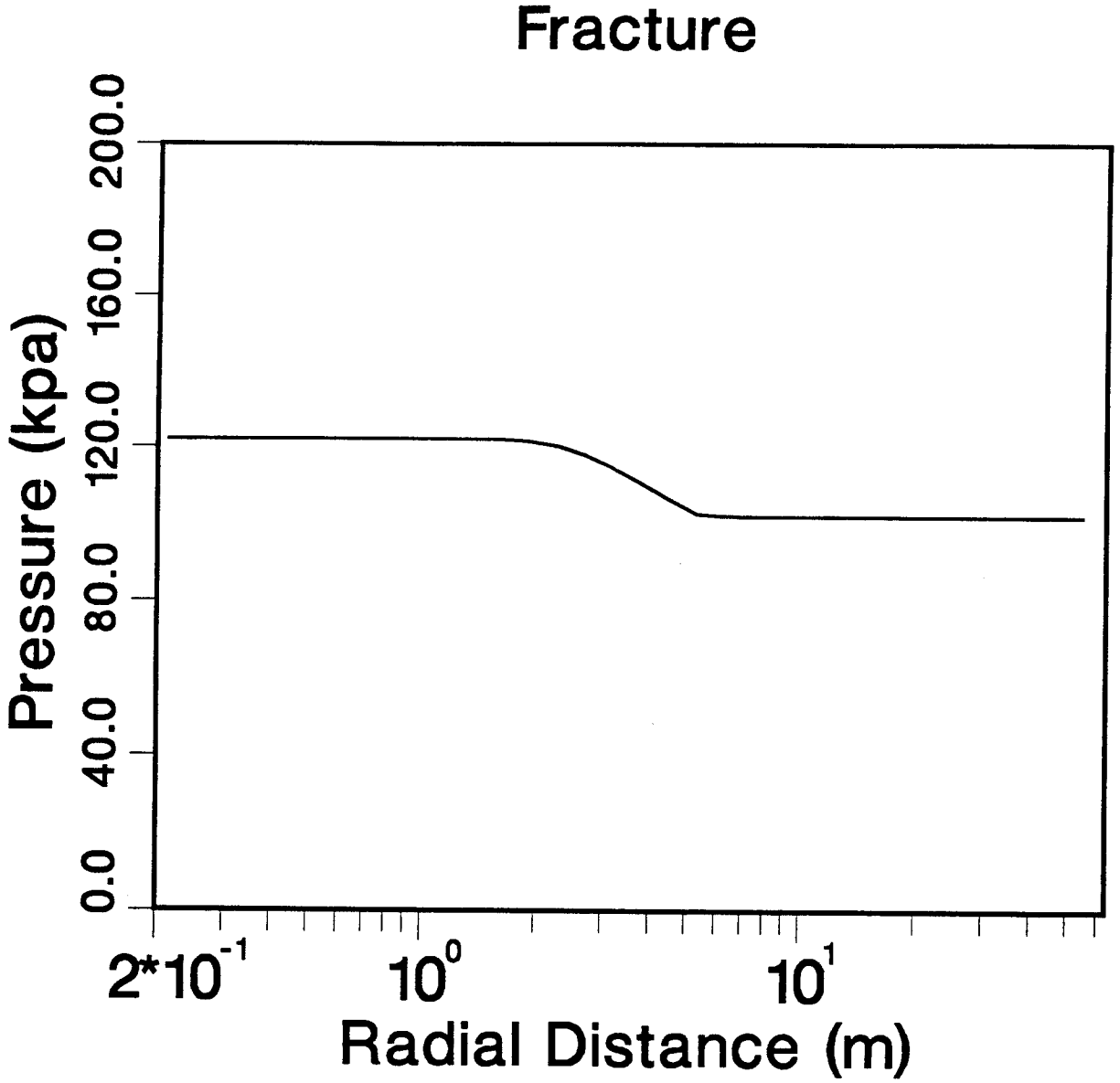

Fracture gas phase pressure, one dimensional fractured rock example.

FIGURE 11

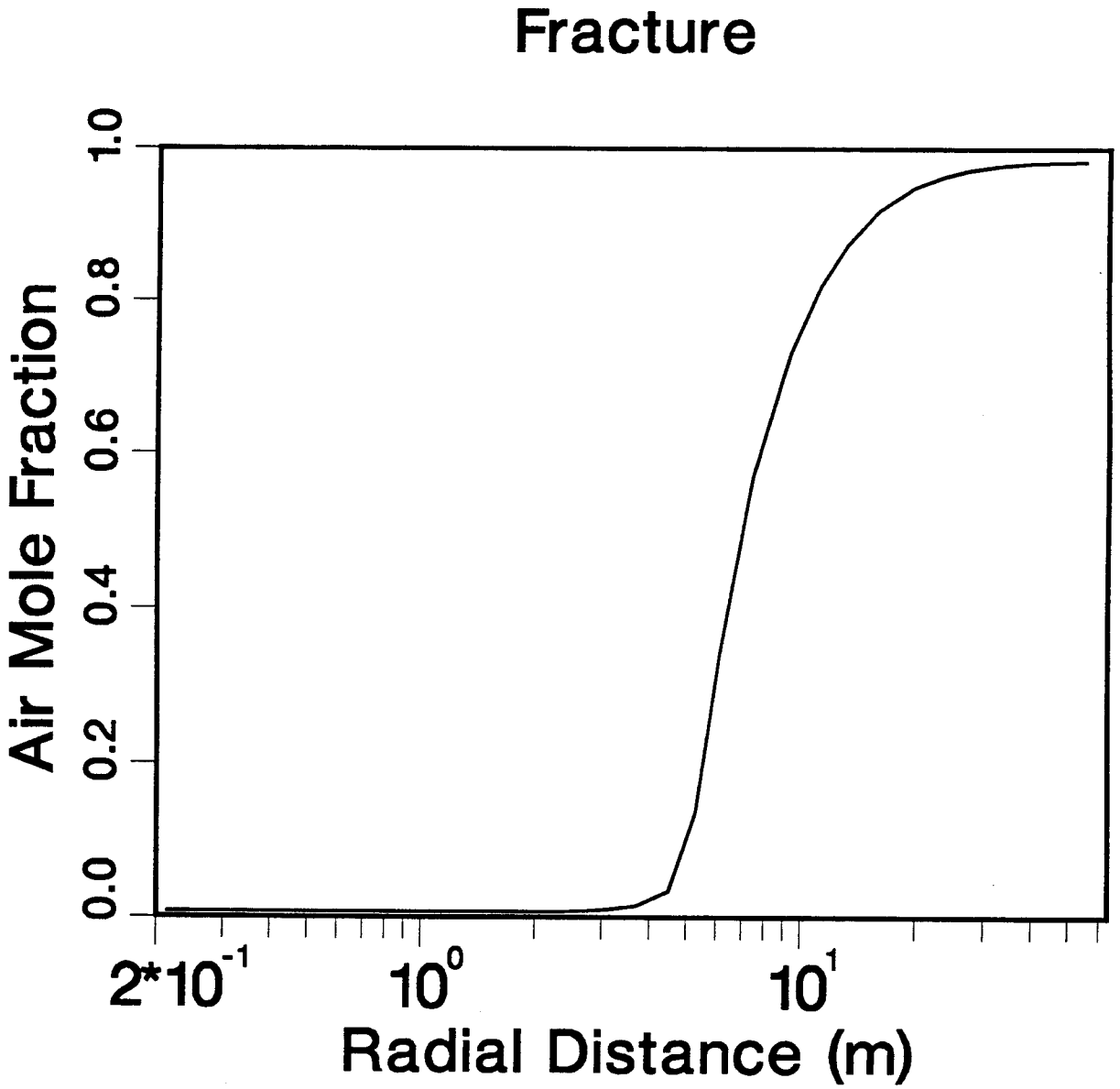

Fracture air mole fraction, one dimensional fractured rock example.

FIGURE 12

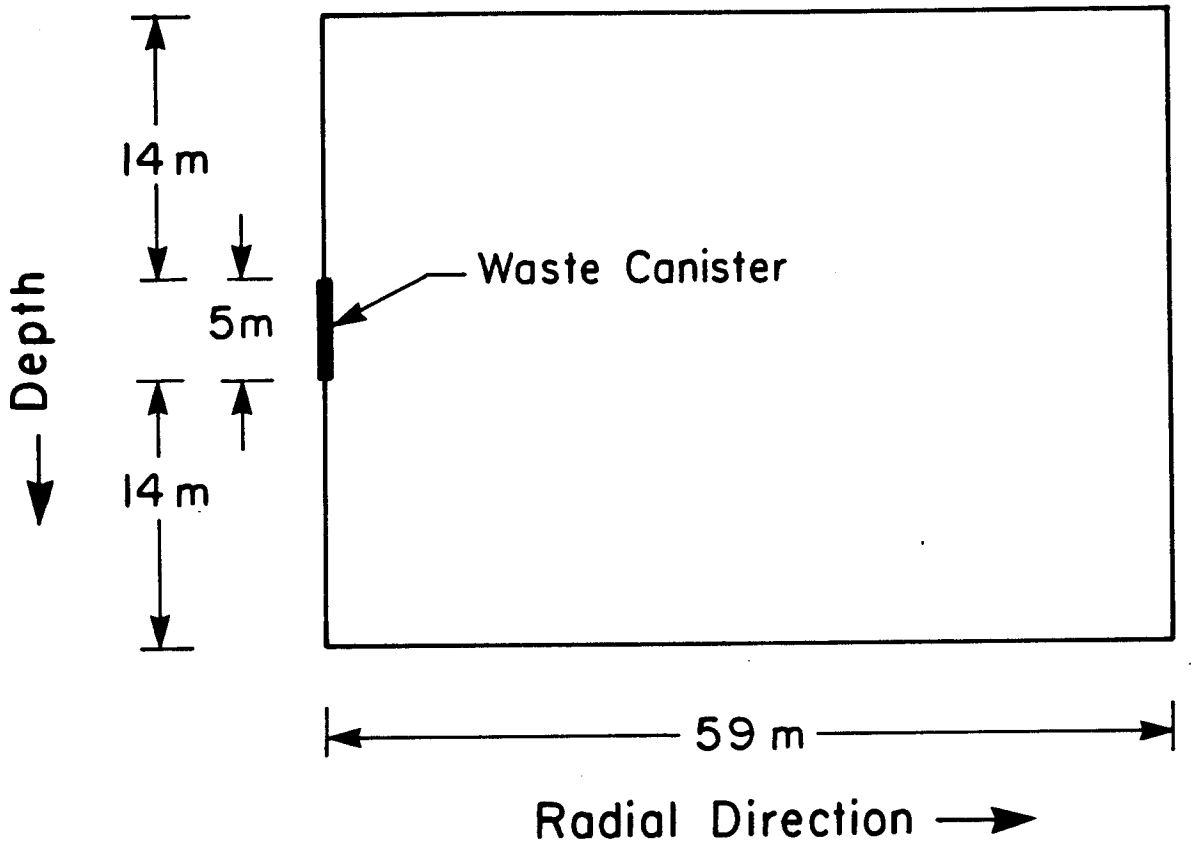

Geometry for two dimensional fractured rock example.

FIGURE 13

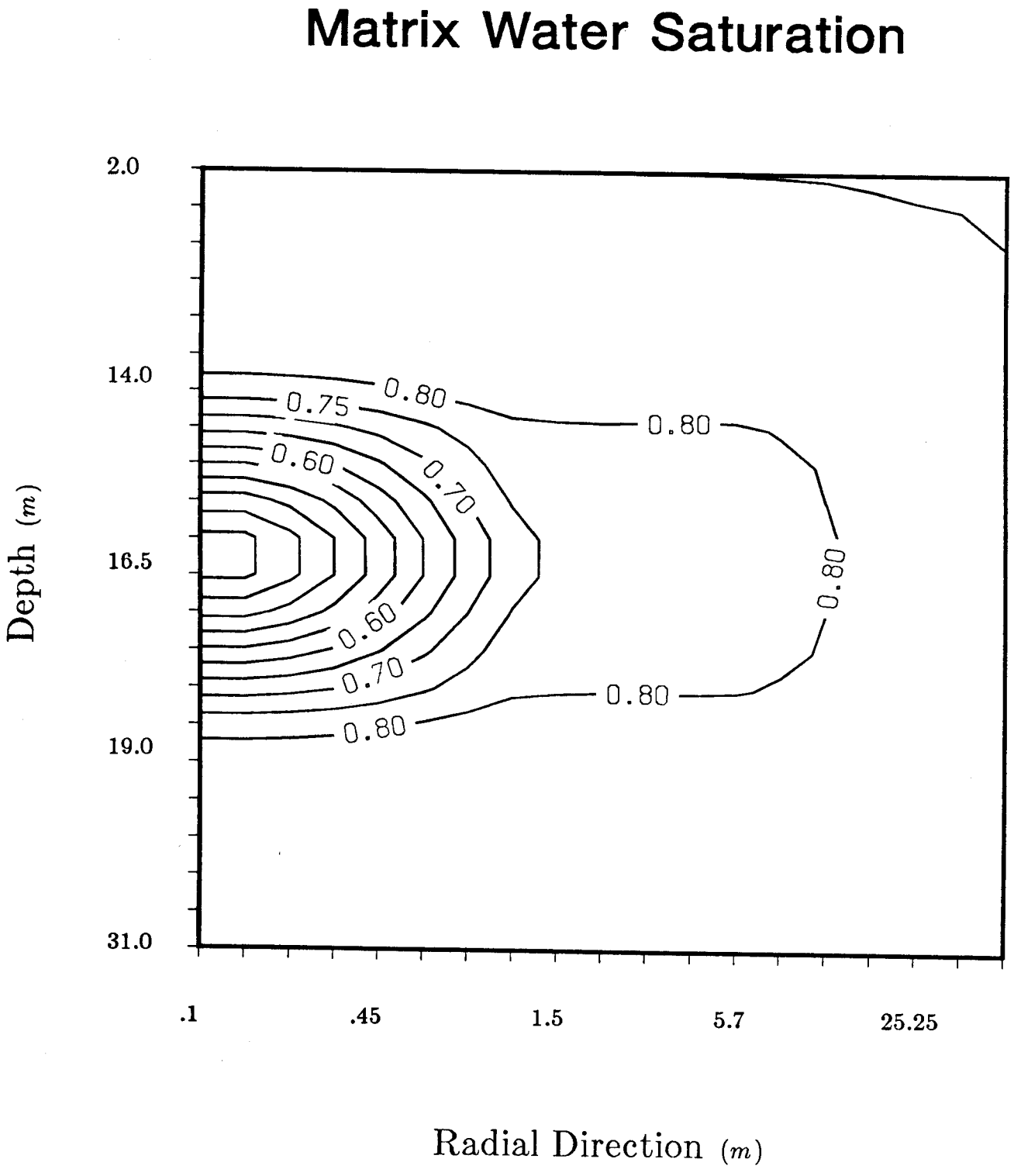

Matrix water saturation, High-P_c case.

FIGURE 14

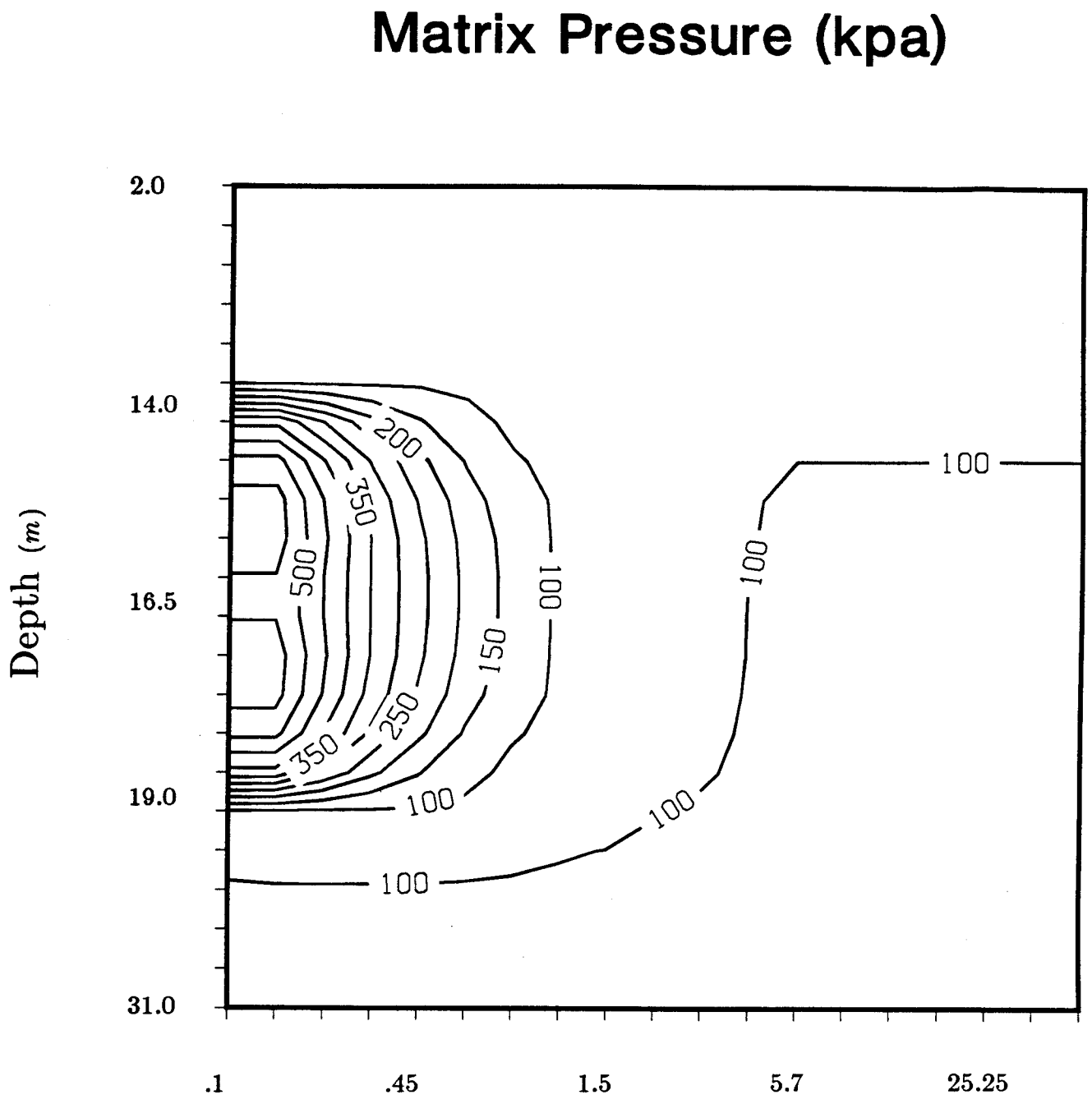

Matrix gas phase pressure, High-P_c case.

FIGURE 15

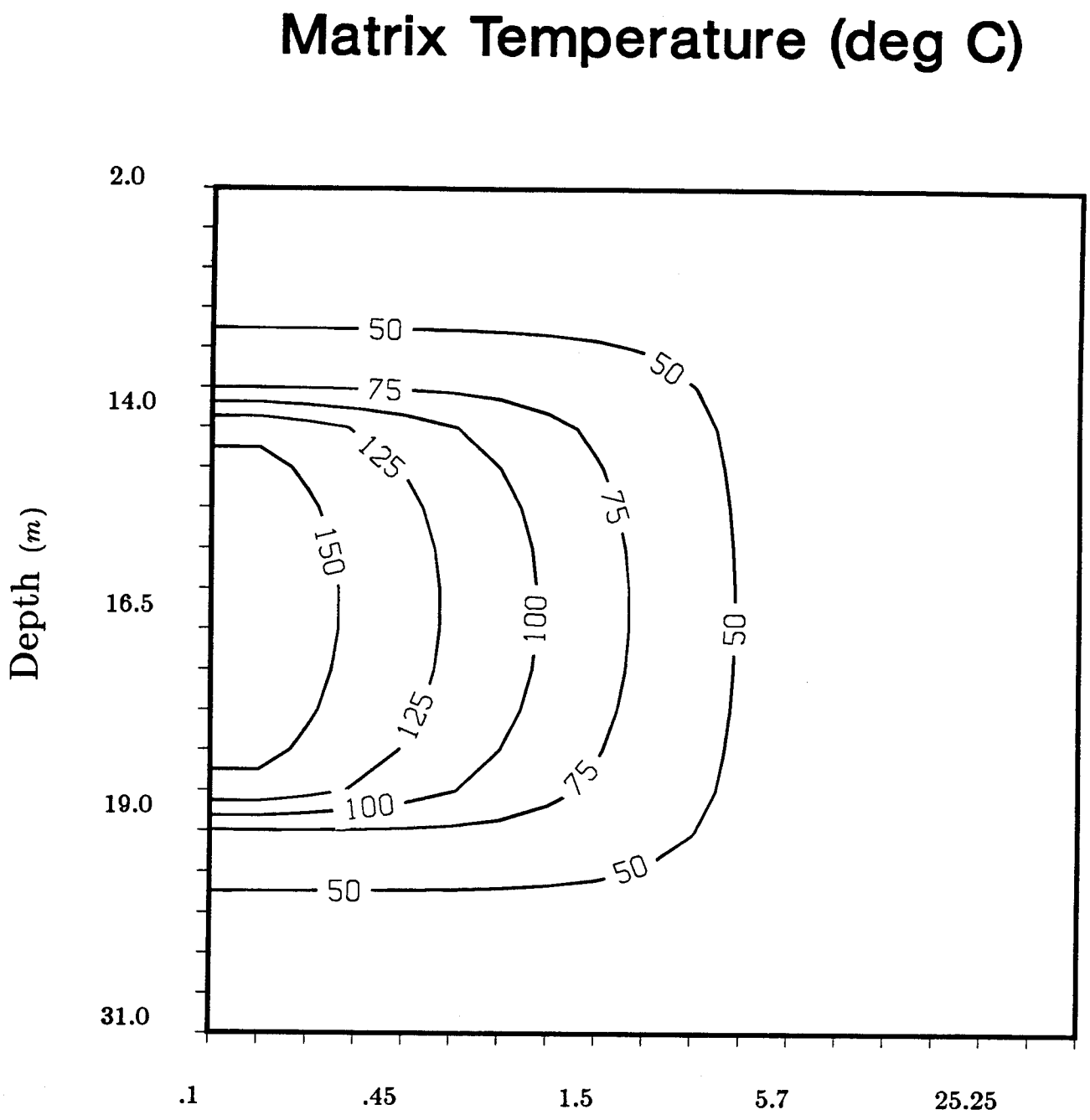

Matrix temperature, fractured rock example, High-P_c case.

FIGURE 16

Matrix Water Saturation

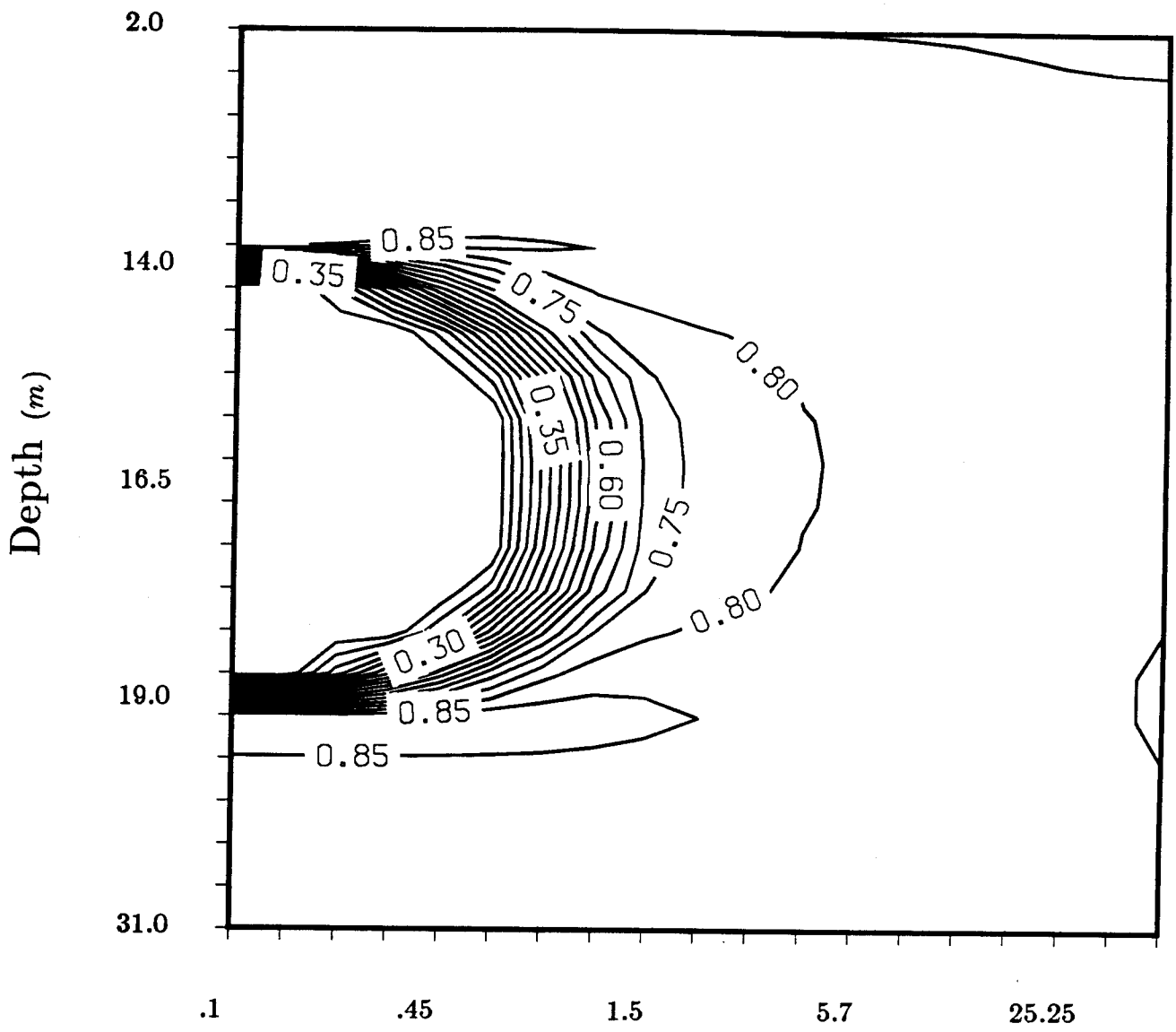

Matrix water saturation, Low-P_c case.

FIGURE 17

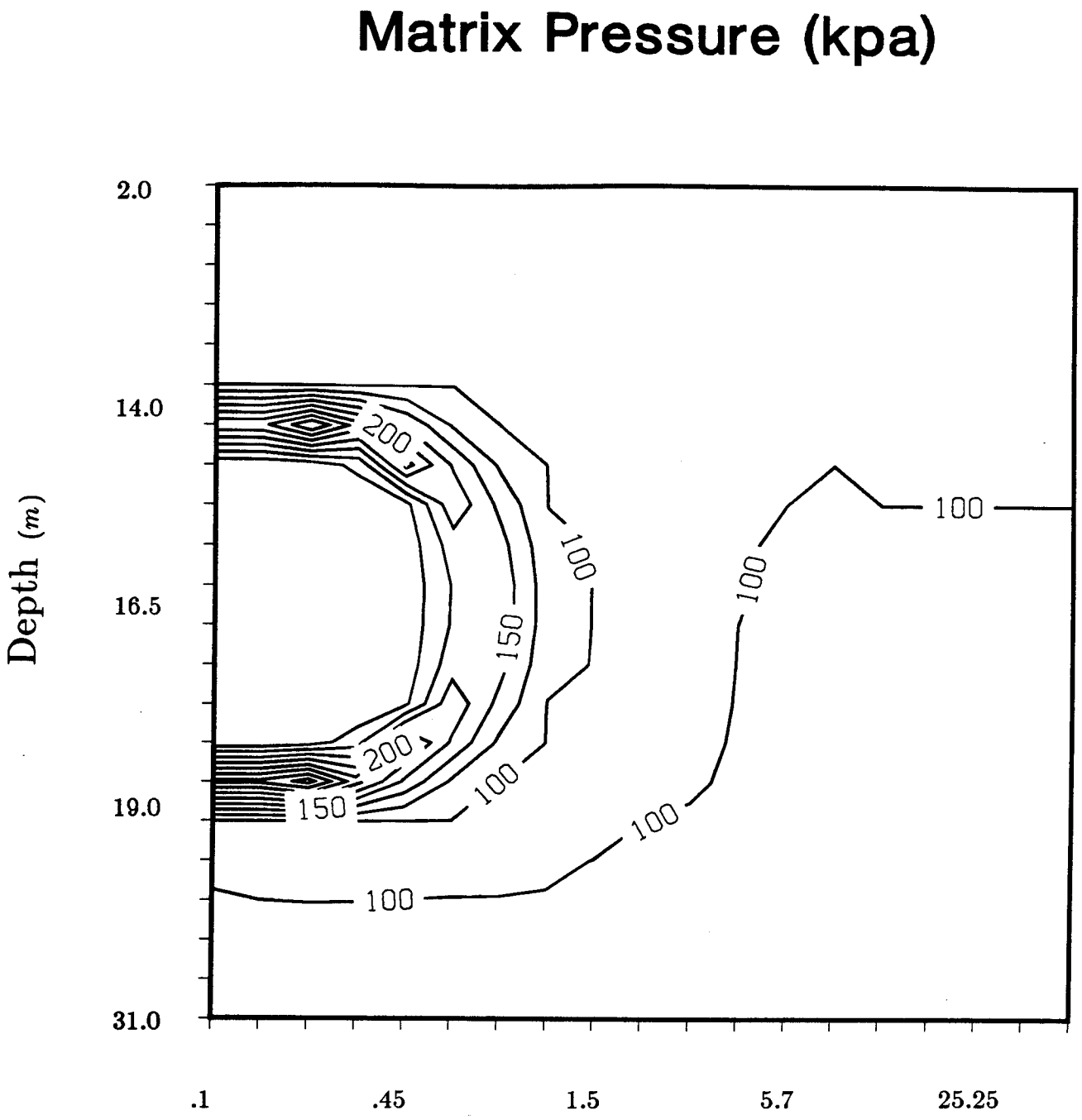

Matrix gas pressure, Low-P_c case.

FIGURE 18

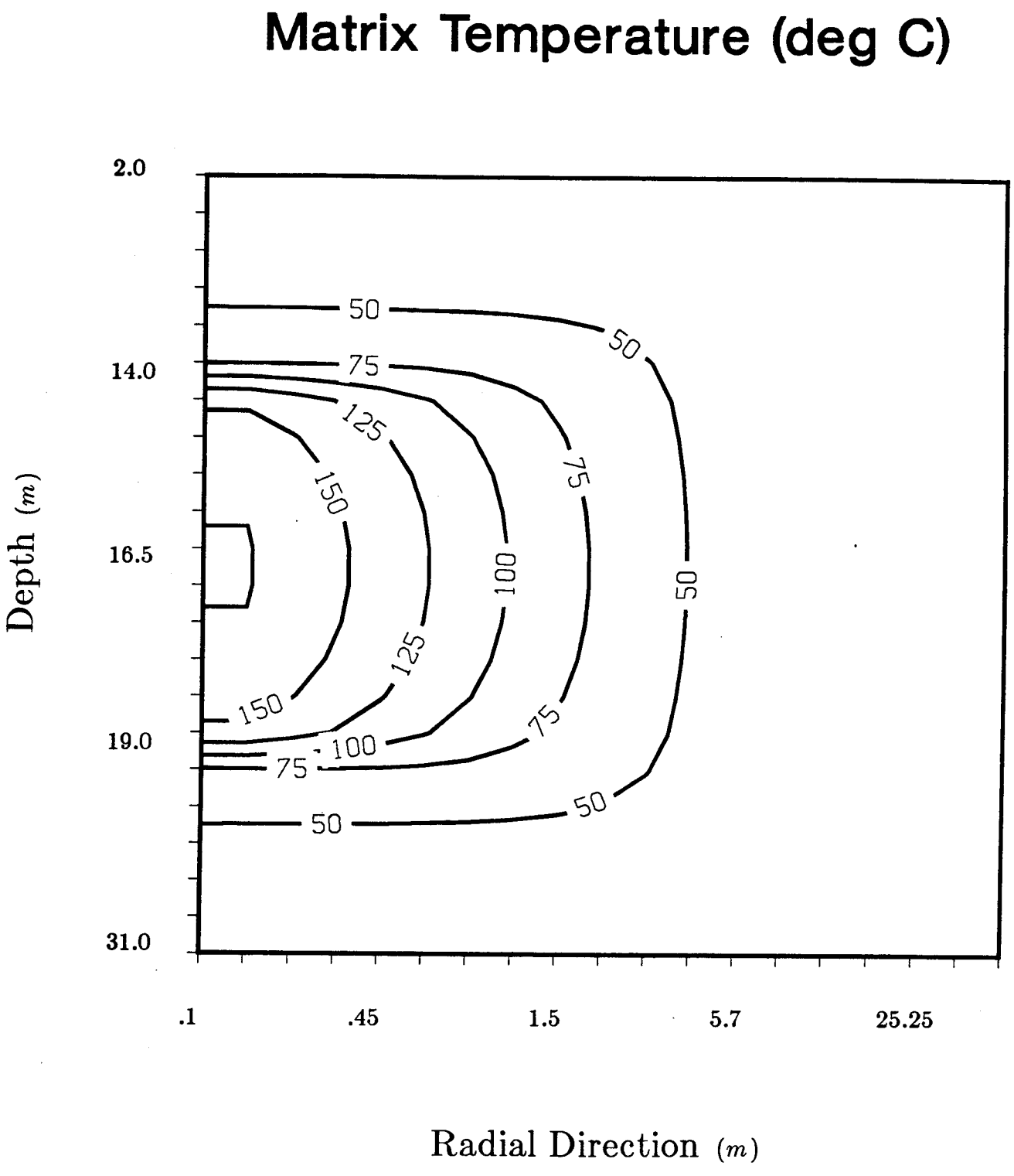

Matrix temperature, Low-P_c case.

FIGURE 19

Matrix Air Mole Fraction

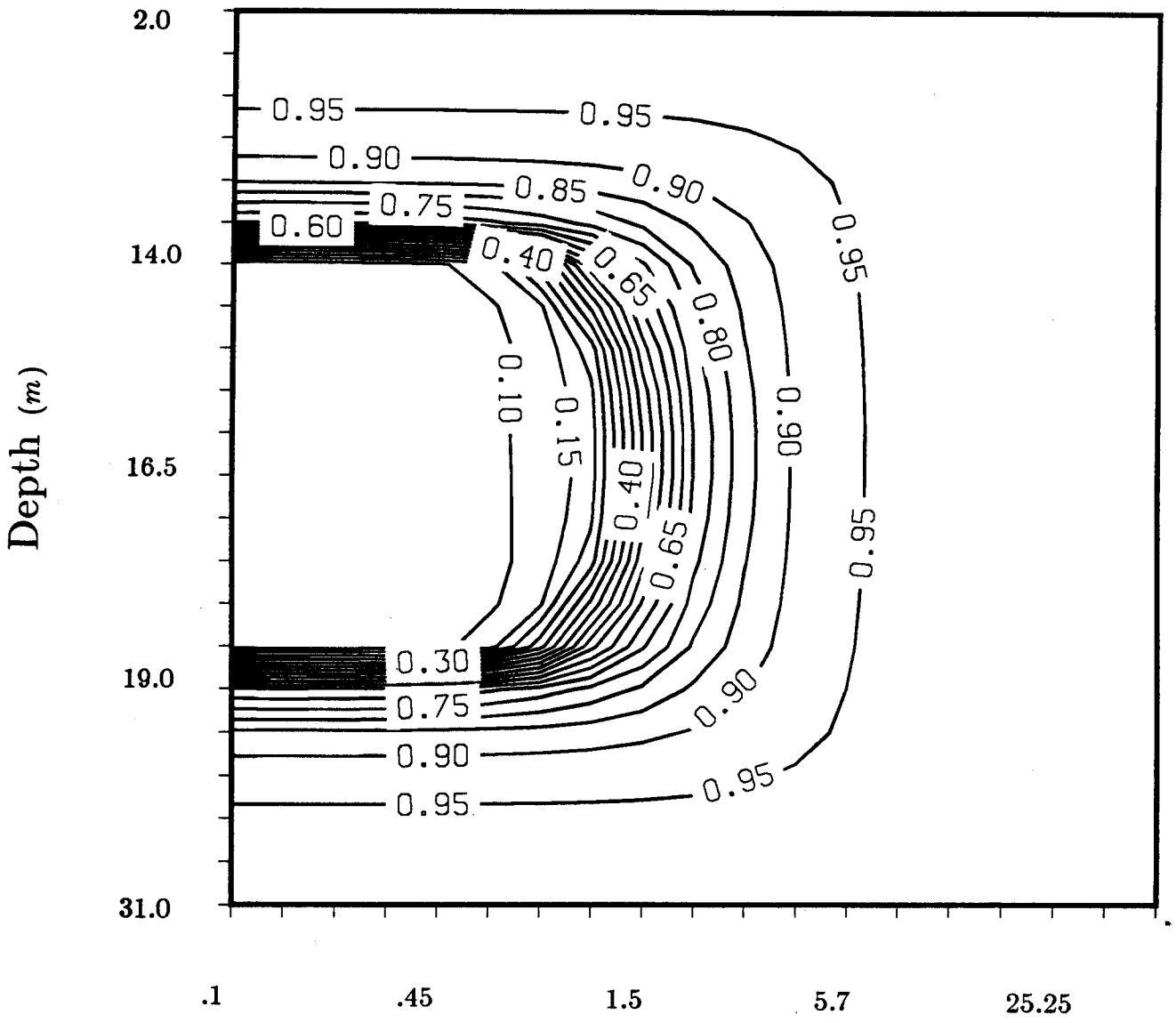

Matrix air mole fraction, Low-P_c case.